AEDC-TR-85-5

Compressor and Turbine Models — Numerical Stability and Other Aspects

K. C. Reddy and Sudheer N. Nayani
The University of Tennessee Space Institute
Tullahoma, TN 37388

April 1985

Final Report for Period May 1, 1982 – May 1, 1984

Approved for public release; distribution unlimited.

ARNOLD ENGINEERING DEVELOPMENT CENTER
ARNOLD AIR FORCE STATION, TENNESSEE
AIR FORCE SYSTEMS COMMAND
UNITED STATES AIR FORCE

APPROVAL STATEMENT

This report has been reviewed and approved.

David A. Duesterhaus

DAVID A. DUESTERHAUS
Directorate of Technology
Deputy for Operations

Approved for publication:

FOR THE COMMANDER

Marion L. Laster

MARION L. LASTER
Director of Technology
Deputy for Operations

UNCLASSIFIED

SECURITY CLASSIFICATION OF THIS PAGE

REPORT DOCUMENTATION PAGE

1a REPORT SECURITY CLASSIFICATION: UNCLASSIFIED

1b RESTRICTIVE MARKINGS:

2a SECURITY CLASSIFICATION AUTHORITY:

2b DECLASSIFICATION/DOWNGRADING SCHEDULE:

3 DISTRIBUTION/AVAILABILITY OF REPORT: Approved for public release; distribution unlimited.

4 PERFORMING ORGANIZATION REPORT NUMBER(S): AEDC-TR-85-5

5. MONITORING ORGANIZATION REPORT NUMBER(S):

6a. NAME OF PERFORMING ORGANIZATION: University of Tennessee Space Institute

6b. OFFICE SYMBOL *(If applicable)*:

7a NAME OF MONITORING ORGANIZATION:

6c. ADDRESS *(City, State and ZIP Code)*: Tullahoma, Tennessee 37388

7b ADDRESS *(City, State and ZIP Code)*:

8a NAME OF FUNDING/SPONSORING ORGANIZATION: Arnold Engineering Development Center

8b OFFICE SYMBOL *(If applicable)*: DOT

9. PROCUREMENT INSTRUMENT IDENTIFICATION NUMBER: F40600-82-C-0003

8c ADDRESS *(City, State and ZIP Code)*: Air Force Systems Command, Arnold Air Force Station, TN 37389

10 SOURCE OF FUNDING NOS

PROGRAM ELEMENT NO.	PROJECT NO.	TASK NO	WORK UNIT NO
65807F			

11 TITLE *(Include Security Classification)*: Please see reverse of this page.

12. PERSONAL AUTHOR(S): Reddy, K.C. and Nayani, Sudheer N., University of TN Space Institute

13a. TYPE OF REPORT: Final

13b. TIME COVERED: FROM 5/1/82 TO 5/1/84

14. DATE OF REPORT *(Yr., Mo., Day)*: March 1985

15 PAGE COUNT: 71

16. SUPPLEMENTARY NOTATION: Available in Defense Technical Information Center (DTIC).

17 COSATI CODES

FIELD	GROUP	SUB GR
12	01	

18 SUBJECT TERMS *(Continue on reverse if necessary and identify by block number)*: mathematical models; compressors; turbines

19. ABSTRACT *(Continue on reverse if necessary and identify by block number)*

This report deals with the mathematical-numerical models used at AEDC for the simulation of compressors and turbines. Numerical stability problems encountered in a one-dimensional compressor model (COMP2SP) have been eliminated with appropriate changes in the algorithm. A multi-dimensional finite volume code (ATAC), which simulates the operation of a turbine, has been analyzed, and the source of numerical oscillations in that code has been isolated. Subsequently, proper changes to the ATAC code have been made at AEDC and numerical oscillations have been eliminated. Stage characteristics based on the total pressure loss coefficient and the deviation angle as functions of incidence angle have been found to be less sensitive to errors in interpolation for intermediate speeds than the pressure and temperature coefficients as functions of the flow coefficient. Multi-dimensional compressor model equations suitable for simulating the circumferentially distorted

20. DISTRIBUTION/AVAILABILITY OF ABSTRACT: UNCLASSIFIED/UNLIMITED ☐ SAME AS RPT ☒ DTIC USERS ☐

21 ABSTRACT SECURITY CLASSIFICATION: UNCLASSIFIED

22a NAME OF RESPONSIBLE INDIVIDUAL: W.O. Cole

22b TELEPHONE NUMBER *(Include Area Code)*: (615)455-2611,x7813

22c OFFICE SYMBOL: DOS

DD FORM 1473, 83 APR — EDITION OF 1 JAN 73 IS OBSOLETE

UNCLASSIFIED

SECURITY CLASSIFICATION OF THIS PAGE

11. TITLE. Continued.

Compressor and Turbine Models - Numerical Stability and Other Aspects

19. ABSTRACT. Continued.

flows have been developed. Characteristics and compatibility equations are derived for the imposition of inflow and outflow boundary conditions.

PREFACE

The work reported herein was conducted at The University of Tennessee Space Institute, Tullahoma, Tennessee and was supported by the Arnold Engineering Development Center under contract number F40600-82-C-0003 for the period May 1, 1982 - May 1, 1984. Technical consultation of Dr. Mitsuru Kurosaka is gratefully acknowledged. The Air Force Project Manager during this contract period was Mr. Dave Duesterhaus, Directorate of Technology.

The reproducibles used in the reproduction of this report were supplied by the authors K. C. Reddy and Sudheer N. Nayani.

CONTENTS

ILLUSTRATIONS

APPENDIXES

1.0 INTRODUCTION

Since it is not feasible to experimentally evaluate an aircraft turbine engine under all possible conditions, mathematical models are built to simulate the operation of the major components of an engine such as the compressor, turbine and combustor which can be tested seperately and together. In this report we are concerned with the mathematical and numerical models of compressors and turbines. The following specific topics are discussed:

1. Numerical stability of a one-dimensional compressor model.
2. Numerical stability of a multi-dimensional finite volume code that simulates a turbine.
3. Stage characteristics used in the compressor models.
4. Multi-dimensional compressor model equations for the simulation of circumferentially distorted flows and their boundary conditions.

Kimzey (Ref. 1) developed a one-dimensional time-dependent model for the analysis of the effects of planar disturbances on a compressor on the basis of conservation laws of mass, momentum and energy. Experimental data are used to synthesize the stage characteristics of the compressor. The compressor stage force and shaft work which are needed in the model are calculated based on these characteristics. The conservation equations are discretized spatially by the use of a two-sided difference scheme. Boundary conditions are imposed on total pressure and total temperature at the inlet boundary and on static pressure or airflow rate at the exit boundary. The resulting system of ordinary differential equations is integrated forward in time by a fourth-order Runge-Kutta scheme.

These models have been applied to a variety of compression systems by Kimzey (Ref. 1) and Chamblee, Davis and Kimzey (Ref. 2). They are used to analyze and extrapolate the experimental data and to study the effects of unsteady disturbances of the aerodynamic stability of the compression system. These models are not always numerically stable. Some of the techniques used for overcoming the numerical instabilities are to increase the friction coefficient in the inlet and exit ducting, to alter the ducting lengths or areas and to time average the numerical solutions once every few time steps. However, these techniques can achieve only conditional numerical stability for some of the compression systems. Also the application of the models has been restricted to limited regions of the operating map, for which they are numerically stable.

Davis (Ref. 1) has applied MacCormack's explicit finite difference scheme to solve the partial differential equations of the model and an approximate version of the method of characteristics to impose the boundary conditions. This scheme is more stable numerically than the earlier method, but this also exhibits numerical oscillations in the solutions under certain conditions. These oscillations are controlled or reduced by the addition of extra friction or dissipation in the inlet duct and by reducing the inlet duct volume. However, the additional extra friction may degrade the accuracy of the simulation of the actual physical system. Davis has applied the one-dimensional compressor model to simulate the dynamics of single spool and dual spool compression systems. The computer code based on this scheme is called COMP2SP in this report for identification purposes.

Reddy and Tsui (Ref. 3) have analyzed the compressor model equations and concluded that the boundary conditions should be imposed accurately based on the method of characteristics (M.O.C.). They have tested various numerical schemes together with the M.O.C. boundary conditions and concluded that MacCormack Scheme provided a reliable and numerically stable method. They have not reported any numerical oscillations mentioned in Ref. 4. The one-dimensional compressor code based on this work is called COMPUT.

One of the topics addressed in this report is the identification of the source of numerical oscillations in the one-dimensional two spool compressor model, COMP2SP and the changes that have been made to remove the numerical oscillations and to enhance the accuracy of the model. This is essentially accomplished by detailed comparisons of the results of COMP2SP and COMPUT for an identical test case, as reported in Section 2.

The ARO-1 code is a three-dimensional, finite volume code for solving the unsteady Euler equations using an explicit MacCormack scheme. This code has been modified at AEDC to simulate a turbine by including source terms, such as the blade force and shaft work. The source terms are computed from the known performance characteristics of the turbine. This is called the ATAC code. Numerical oscillations were observed in the solutions of this code in and around the turbine. In order to analyze this problem, a turbine version of the COMPUT code has been developed and it did not produce any numerical oscillations. From detailed comparisons it has been found that the source of oscillations in the ATAC code was the manner in which the source terms were incorporated into the algorithm. As reported in Section 3, appropriate changes have been made to the ATAC code which remove the spurious oscillations. Some transient flow results based on the one-dimensional turbine code have also been reported.

The compressor model equations typically depend on various stage characteristics. These are obtained experimentally at great expense and can be done only for some discrete rotational speeds. Intermediate stage characteristics have to be obtained based on some interpolation techniques. It is necessary to develop some rational models for various stage performance characteristics in order to interpolate for intermediate speeds. The compressor models developed at AEDC have traditionally used the stage characteristics based on curves representing the pressure coefficient, ψ_p and temperature coefficient, ψ_t as functions of the flow coefficient, ϕ for various corrected speeds. Polynominal surface fits for interpolating the stage characteristics for intermediate corrected speeds have been found to be unsatisfactory. We report a study of using alternate stage characteristics which may be interpolated better for intermediate speeds. In Section 4, a calculation procedure based on the total pressure loss coefficient, $\bar{\omega}$ and the deviation angle, δ as functions of the angle of incidence, i and corrected speed is outlined. Based on test results, stage characteristics based on $\bar{\omega}$ and δ as functions of i are less sensitive to errors in interpolation for intermediate speeds than ψ_p and ψ_t vs ϕ.

Multi-dimensional compressor models are necessary for studying the effects of distortion in the inlet flow and other non-uniformities in the flow field such as the rotating stall on the compressor operation. In Section 5, unsteady two-dimensional compressor model ($z - \theta$ model) equations have been developed and analyzed. This is a radially averaged model suitable for circumferentially distorted flows. Characteristics and compatibility equations which can be used to impose the inflow and outflow boundary conditions accurately, have been developed. These equations are developed in a form suitable for developing a two-dimensional compressor code using similar numerical techniques as those used in one-dimensional codes.

2.0 ONE-DIMENSIONAL COMPRESSOR MODEL

As discussed in the last section, the one dimensional two spool compressor model, developed at AEDC, exhibited numerical oscillations under some conditions and was unstable under some other conditions. For identification purposes we name the computer code for this model as COMP2SP in this report. We describe in this section the changes that have been made to COMP2SP to remove the numerical oscillations and instability and to enhance the accuracy of the model. The source of numerical oscillations in COMP2SP was identified by comparing the results of this code with the results of a one-dimensional single spool compressor model developed earlier at UTSI, which we name COMPUT, for an identical test case. The test case run was for a ten stage compressor operating at 87 percent corrected speed. A brief description of the salient features of the two models is given below, followed by the changes made to COMP2SP and the results.

2.1 COMPUT (SINGLE SPOOl)

The governing equations are derived (Refs. 1 and 2) by the application of the mass, momentum and energy conservation laws to an elemental control volume in which the blade forces, wall shear forces, shaft work done, heat added to the fluid and mass bleed flow rate are included. The resulting system of first order partial differential equations can be written as follows:

$$\frac{\partial \vec{u}}{\partial t}(z,t) + \frac{\partial \vec{f}}{\partial z}(\vec{u}) + \vec{g}(\vec{u},z,t) = 0 \tag{1}$$

where,

$$\vec{u}(z,t) = \begin{bmatrix} \rho A \\ \rho A U \\ \rho A(e + \frac{U^2}{2}) \end{bmatrix} \quad , \quad \vec{f}(\vec{u}) = \begin{bmatrix} \rho A U \\ A(\rho U^2 + P) \\ \rho A U C_p T_t \end{bmatrix}$$

$$\vec{g}(\vec{u},z,t) = \begin{bmatrix} W_B \\ -P\frac{\partial A}{\partial Z} - F \\ -W_s - Q \end{bmatrix} = \begin{bmatrix} g_1 \\ g_2 \\ g_3 \end{bmatrix} \tag{2}$$

The various symbols represent the following:

ρ - density
A - area
U - axial velocity
e - internal energy
P - static pressure
C_p - specific heat at constant pressure
T_t - stagnation temperature
W_B - compressor bleed flow rate
F - force of compressor blading and casing friction acting on the fluid
W_s - stage shaft work added to fluid in control volume
Q - rate of heat addition to control volume

In conjunction with the partial differential Eq. (1), we have the equation of state given by,

$$P = \rho RT \tag{3}$$

where T is the static temperature and R the gas constant. In addition we have the equations relating the internal energy and stagnation temperature to other variables as follows:

$$e = C_p T/\gamma \tag{4}$$

$$C_p T_t = C_p T + \frac{U^2}{2} \tag{5}$$

The area distribution $A(z)$ is known for a given compressor system. In the vector $\vec{g}$, which acts like a forcing function in the differential equation, various terms are modeled empirically for a particular compressor. $F(z,t)$ represents the forces of the blades and the casing friction acting on the fluid. In practice it is difficult to isolate $F(z,t)$ empirically from the experimental data and hence the total term $(F + P\frac{\partial A}{\partial z})$ which represents the forces including the wall pressure area force is modeled from the experimental data. $W_s(z,t)$ is the shaft work done on the fluid, which is calculated from the stage characteristics of the compressor. The stage characteristics are modeled empirically based on experimental measurements of stage total temperature, flow rate, total pressure and flow angularity at the stage entry and exit.

In Ref. 3, various numerical schemes for integrating these equations and their stability characteristics have been analyzed. It has been concluded that McCormack scheme together with the method of characteristics (M.O.C) boundary conditions is more accurate and reliable than other schemes tried in predicting the compressor surge. With this scheme no numerical instabilities have been encountered.

In Ref. 3. the following compatibility equations along the three characteristics of the system of Eq. (1) have been derived.

$$c^2 \frac{d\bar{\rho}}{dt} - \frac{d\bar{P}}{dt} + c^2 \breve{g}_1 - \breve{g}_3 = 0 \quad \text{along } \frac{dz}{dt} = U \tag{6}$$

$$\bar{\rho} c \frac{dU}{dt} + \frac{d\bar{P}}{dt} + \bar{\rho} c \breve{g}_2 + \breve{g}_3 = 0 \quad \text{along } \frac{dz}{dt} = U + c \tag{7}$$

$$-\bar{\rho} c \frac{dU}{dt} + \frac{d\bar{P}}{dt} - \bar{\rho} c \breve{g}_2 + \breve{g}_3 = 0 \quad \text{along } \frac{dz}{dt} = U - c \tag{8}$$

where, $\bar{\rho} = \rho A, \bar{P} = PA$ and

$$\begin{bmatrix} \breve{g}_1 \\ \breve{g}_2 \\ \breve{g}_3 \end{bmatrix} = \begin{bmatrix} g_1 \\ \frac{U}{\bar{\rho}} g_1 - \frac{1}{\bar{\rho}} g_2 \\ \frac{(\gamma-1)}{2} U^2 g_1 - (1-\gamma) U g_2 + (\gamma - 1) g_3 \end{bmatrix} \tag{9}$$

where g_1, g_2 and g_3 are given by Eq. (2). For subsonic flows, two boundary conditions are imposed at the left boundary. Typically, the total pressure $P_t(t)$ and total temperature $T_t(t)$ are prescribed at the inflow boundary. These two boundary conditions and the compatibility Eq.(2.8) are solved to obtain all the flow variables at the inflow boundary, which are necessary for the interior point numerical scheme. Similarly, one boundary condition, say, the prescription of the static pressure $P(t)$ at the outflow boundary and the two compatibility Eqs. (6) and (7) along the out-going characteristics are sufficient to compute all the variables at the outflow boundary. Details of this scheme are given in Ref. 3.

2.2 COMP2SP (TWO SPOOL)

The one-dimensional compressor modeling technique has been extended to include dual-spool compression systems of the type shown in Fig. 1. and has been applied to a 13-stage compression system by Davis in Ref. 4. Variable compressor inlet geometry is used on both the fan and high pressure compressor and is scheduled as a function of airflow, which is determined from compressor inlet temperature and compressor rotor speed. Stage characteristics necessary for model construction were based on experimental data. High pressure compressor characteristics were the same as those used in the single spool model. Fan characteristics were synthesized from the fan rig data.

COMP2SP differs mainly from COMPUT, in the boundary treatment. In Ref. 4, ignoring the viscous forces and conduction heat transfer along the characteristic curves, the compatibility equations were derived to be,

$$dP - \rho c dU = 0 \text{ for } \frac{dz}{dt} = U - c \tag{10}$$

$$dP + \rho c dU = 0 \text{ for } \frac{dz}{dt} = U + c \tag{11}$$

Inlet Boundary Solution: The inlet thermodynamic properties for any time can be calculated by specifying certain boundary conditions (P_t and T_t) and using the characteristic relationships of Eq. (10). The characteristic equation is first solved by approximating the total derivatives by differences,

$$z_{new} - z_I = (U - c)\Delta t \tag{12a}$$

Figure 2 shows the determination of the intersection of the characteristic curve (point z_I) with the geometry of the previous time step (line AB). The thermodynamic relationships at point z_I can be determined by linear interpolation of the properties between points A and B. Once this point is known, the compatibility Eq. (10) can be approximated by differences

$$P_{z_{new}} - P_{z_I} = \rho c (U_{z_{new}} - U_{z_I}) \tag{12b}$$

An iterative technique is employed to solve Eq. (12b) along with the boundary conditions that P_t and T_t are prescribed. To obtain a more accurate value of $P_{z_{n,w}}$, an outer iteration is applied to Eq. (10), with density and acoustic velocity now being an average between the interpolated value in the old time frame and the previous iterated value at the new time step. All thermodynamic properties are calculated using these relationships and equation of state.

Exit boundary solution: For subsonic exit conditions, static pressure is specified as the exit boundary condition. A characteristic scheme similar to the one used at the inlet boundary can be employed. In addition to using the characteristic relationships of Eq. (11), the third characteristic equation along a streamline is also used.

$$dP - c^2 d\rho = 0 \quad \text{for} \quad \frac{dz}{dt} = U \tag{13}$$

A procedure similar to the inlet solution procedure is used with each compatibility equation solved along its characteristic curve or streamline curve as shown in Figure 3. With the specification of static pressure and the two compatibility equations, iterative procedure is not needed in this case. It may be noted that the Eqs. (2.14), (13) and (11) are approximations of the more general Eqs. (6), (7) and (8), respectively.

2.3 MODIFICATIONS MADE TO COMP2SP

The following modifications were made to the COMP2SP code to remove numerical oscillations and instabilities.

1. An arithmetic error in the subroutine FRICFZ, which computes friction forces in the duct volumes, is corrected.
2. The flow variables in the FORCES subroutine, which computes the force terms for compressor volumes, are updated after the predictor step of the finite difference scheme, in addition to updating them after the corrector step. Also, friction forces in the last duct volume are included in the scheme which was not done in the original code.
3. Accurate boundary conditions are imposed based on the method of characteristics at both inflow and outflow boundaries using Eqs. (6), (7) and (8) as was done in COMPUT code.

With change 1, COMP2SP does not exhibit numerical oscillations and yields stable calculations as shown in Figs. 4 and 5 for 400 time steps.

Figures 6 and 7 show the calculations of COMP2SP with changes 1 and 2. They are also stable and are almost identical to Figs. 4 and 5.

Figures 8 and 9 show the calculations of COMP2SP with changes 1, 2, and 3. They show that the flow reaches stable steady asymptotic state in only 300 time steps. These results are slightly more accurate than those of Figs. 4-7, as can be expected by the more accurate boundary conditions. With these changes COMP2SP becomes identical to COMPUT in a single spool case.

3.0 TURBINE MODELING

A general three-dimensional, finite volume code that solves unsteady Euler equations using an explicit MacCormack scheme has been modified at AEDC to simulate a turbine by the addition of appropriate forcing functions and by the introduction of proper geometry and boundary conditions. The forcing functions are calculated based on turbine stage characteristics which are input as data. This turbine modeling code is named the ATAC code. The testing of this code has been carried out in one-dimensional mode. In one-dimensional simulation of a single stage turbine the code has exhibited non-physical numerical oscillations. We have analyzed the source of these oscillations by comparing the results of the ATAC code with the results of a turbine version of our one-dimensional finite difference code (COMPUT), which we name TURBUT. The source of the spurious oscillations in ATAC code has been identified to be in the calculation of the forcing functions. This section describes the details of the calculation procedures for the forcing functions in both TURBUT and ATAC codes and the changes made in ATAC to remove the numerical oscillations. We also report some results obtained by TURBUT under transient flow conditions in a turbine.

The source terms are computed as functions of Mach number from the known performance characteristics of the turbine. In the test case, a single stage turbine is divided into eight equal volumes. The computational region is a long constant area duct extending from -5.7 to 5.9 ft. The turbine inlet is at 0.0 ft and the outlet is at 0.2 ft. The entire duct is divided into 80 control volumes.

Initially the flow is assumed to be uniform from the inlet of the duct to the inlet face of the turbine, and from the exit face of the turbine to the duct outlet. The flow through the turbine is computed from the performance characteristics. Starting from these initial conditions, the ATAC code is run at AEDC for 4800 time steps, at a CFL number of 0.8. The steady state distribution of density, mass flux and Mach Number with axial distance are shown in Figs. 10-12. As can be seen the oscillations in these profiles are localized. just inside and near the turbine inlet and outlet. and hence could not be attributed to any problems at the boundaries. Further. the initial inlet Mach Number to the turbine, which is close to the final steady state value, had to be held fixed during the calculations. When the inlet Mach number was allowed to vary with time, the code became unstable in a few time steps.

In order to solve this problem, a one-dimensional compressor code, COMPUT described in the previous section has been modified to handle the turbine performance characteristics. The modified code is called TURBUT. This is a finite difference code which uses an explicit, predictor-corrector, MacCormack scheme. When the code is run for 4,800 time steps, there is no evidence of oscillations in the flow variables, as can be seen from Figs. 13-15. The cause of the oscillations in ATAC code is traced to the manner in which the source terms are handled in that code.

3.1 FORCE FUNCTIONS IN THE FINITE DIFFERENCE SCHEME (TURBUT)

For a specific turbine volume, knowing the inflow conditions and the stage characteristics, the outflow conditions can be calculated. The differences between the outflow and inflow values of impulse functions give the forces and the shaft work. How the blade forces are included in the momentum equation is described below. Suppose the computation is at the node i. Using the flow conditions at $(i-1)$ station as inflow variables, outflow variables at the end of a single turbine volume (station i) can be computed using the turbine stage characteristics. The force function at the (i-1) station is given by

$$g_2(i-1) = IMP_{in} - IMP_{out}$$

where,

IMP_{in} = impulse function defined as, $A(\rho u^2 + p)$ calculated at station $(i-1)$

IMP_{out} = Impulse function calculated from stage characteristics at station i

Consider the momentum equation,

$$\frac{\partial}{\partial t}(\rho A U) = -\left\{\frac{\partial}{\partial z}[A(\rho U^2 + P)] + g_2\right\}$$
$$= -\left\{\frac{\partial}{\partial z}(IMP) - g_2\right\}$$

For point i, the predictor step becomes,

$$\frac{\partial}{\partial t}(\rho A U)\Big|_i = -\left[\frac{IMP(i) - IMP(i-1)}{\Delta z} + \frac{g_2(i-1)}{\Delta z}\right]$$
$$= -\frac{1}{\Delta z}\left[IMP(i) - IMP(i-1) - (IMP_{out} - IMP_{in})\right]$$

$IMP_{in} = IMP(i-1)$ and in the steady state, $IMP_{out} = IMP(i)$ so that the time derivative is zero. However. in general $IMP_{out} \neq IMP(i)$

For the corrector step we have,

$$\frac{\partial}{\partial t}(\rho A U)\Big|_i = -\left[\frac{IMP(i+1) - IMP(i)}{\Delta z} + \frac{g_2(i)}{\Delta z}\right]$$

$$= -\frac{1}{\Delta z}\left[IMP(i+1) - IMP(i) - (IMP_{out} - IMP_{in})\right]$$

Once again, $IMP_{in} = IMP(i)$ and for the asymptotic steady state condition, $IMP_{out} = IMP(i+1)$, so that the time derivative vanishes only in the asymptotic steady state.

Thus proper switching of the index for the source terms in the predictor and corrector steps gives the correct steady state values.

3.2 FINITE VOLUME SCHEME (ATAC)

The finite volume scheme approximates the governing equations

$$\frac{\partial \vec{u}}{\partial t} + \nabla \cdot \vec{f} + \vec{g} = 0$$

in integral form over a control volume V.

$$\frac{\partial}{\partial t}\int_V \vec{u}dV + \int_V \nabla \cdot \vec{f}dV + \int_V \vec{g}dV = 0$$

The numerical solution algorithm used to solve the above system of equations is an explicit predictor-corrector scheme.

For predictor,

$$\hat{u}^{N+1} = u^N + \omega\Delta t\left[-\frac{1}{V}\left(\sum_k f_k \cdot s_k^+ + \sum_k f_k^- \cdot s_k^-\right) - g\right]$$

For corrector,

$$u^{N+1} = \frac{1}{2\omega}\hat{u}^{N+1} + \left(1 - \frac{1}{2\omega}\right)u^N + \frac{\Delta t}{2}\left[-\frac{1}{V}\left(\sum_k \hat{f}_k^+ \cdot s_k^+ + \sum_k \hat{f}_k \cdot s_k^-\right) - \hat{g}\right]$$

Consider the approximation for the axial momentum equation applied to a one-dimensional control volume V_i for illustrating the detail.

<u>Predictor:</u>

$$\frac{\partial}{\partial t}(\rho AU)\mid_i = -\frac{1}{\Delta z}\left[IMP(i) - IMP(i-1) + g_2(i-1)\right]$$

where,

$$g_2(i-1) = IMP_{in} - IMP_{out}$$
$$IMP_{in} = IMP(i-1)$$
$$IMP_{out} = IMP \text{ Computed based on stage characteristics for volume } i$$

<u>Corrector:</u>

$$\frac{\partial}{\partial t}(\rho AU)\Big|_i = -\frac{1}{\Delta z}\left[IMP(i+1) - IMP(i) - g_2(i)\right]$$

where,

$$g_2(i) = IMP_{in} - IMP_{out}$$
$$IMP_{in} = IMP(i)$$
$$IMP_{out} = IMP \text{ computed based on stage characteristics for volume (i+1)}$$

The above description of the force calculation in the corrector step of the finite volume scheme is the modified version in the ATAC code. In the earlier version of the corrector, the force calculation for V_i was based on flow conditions in V_i as inflow conditions for V_i, which was making the scheme to produce spurious numerical oscillations.

Subsequently, the corrector setp has been modified in such a way that the force on V_i is based on flow conditions at V_i going into V_{i+1}, which makes the scheme stable and remove the spurious oscillations. It may be noted that in the modified version, time derivatives go to zero in the asymptotic steady state as they should. Modified ATAC code in one-dimensional case now produces the same results as the one-dimensional code TURBUT.

3.3 STUDIES OF TRANSIENT FLOW CONDITIONS IN A TURBINE

In order to study the effects of transient flow conditions on a turbine, the code TURBUT was run with changes in the static pressure at the exit.

Computation was started with steady state flow conditions at the time step 6600, established in an earlier run. At that time the static pressure at the outflow plane of the exit duct was impulsively dropped from 9.485 psi to 8 psi. By 12,600 time steps, i.e., in an additional 6,000 time steps the flow reached a new steady state condition. The time step used was 0.000015 sec, with the Courant number 0.8. Figures 16 and 17 show the plots of static presure, and mass flow, at various time steps in the duct which has the turbine volumes located between 0 and 0.2 units. It was noticed that for several hundred time steps most of the transient phenomena was limited to the exit duct, which eventually propagated into the inlet duct as well. The Mach number and mass flow in the exit duct underwent strong transient perturbations, and not as much in the inlet duct, before settling down to new steady state conditions compatible with the pressure at the exit plane of the duct. The turbine seems to act like a big damper in not letting the large perturbations of the exit duct go upstream into the inlet duct. It was also noted that the head of rarefaction wave propagated at a speed close to the propagation speed of a small disturbance.

The above experiment was repeated with a sudden increase in exit pressure from 9.485 psi to 10 psi. As before, computation was started with steady state flow conditions, at the time step 6600. At that time the static pressure at the outflow plane of the exit duct was impulsively increased to 10 psi and held fixed. The relative magnitude of the pressure pulse was 0.054. In an additional 4,500 time steps the flow had reached a new steady state condition. Figure 18 is a plot of the non-dimensional static pressure in the duct at various time steps. The CFL number for this computation was 0.8.

The next set of experiments consisted of introducing a compression wave followed by a rarefaction wave. This was accomplished by impulsively increasing the exit pressure from

9.485 psi to 10 psi, holding it fixed for 100 time steps, and then dropping it back to 9.485 psi. Figure 19 is a plot of static pressure vs distance downstream of the turbine exit at various time steps. At the time step 6600, the exit pressure was increased to 10 psi and held fixed for 100 time steps. At the time step 6700, the exit pressure was dropped back to 9.485 psi and held fixed thereafter. This set up a pressure pulse travelling up the duct. The amplitude of the pressure pulse was 0.415 psi. Figure 20 is similar to Fig. 19 with plots drawn at closer time intervals. The wave speed, obtained from Fig. 20 by calculating the time it takes for the peak of the pulse to travel from one location to another, is 828 fps. This value agrees well with the local $(U - c)$ value (acoustic propagation speed) of 838 fps that exists at the peak of the wave.

The leading edge of the pressure pulse hits the exit face of the turbine at the time step 7000 (t = 0.006 sec), and is almost instantaneously transmitted through the turbine. It may be noted that the turbine extends a distance of only 0.2 units. The propagation of the wave that is transmitted upstream through the turbine is shown in Fig. 21. The amplitude of the wave is 0.121 psi. While the amplitude of the transmitted wave is reduced, the propagation speed increases gradually from the 828 fps to the local acoustic speed of 924 fps in the upstream duct.

Figure 22 is a plot of the static pressure versus distance in the downstream portion of the duct for $N > 7000$. where N is the number of time steps. The effect of the multiple reflections of the pulse at the turbine exit face and the exit of the duct on the pressure distribution can be clearly seen. As can be seen from the $N = 7400$ values, the flow will settle to the correct steady state value.

4.0 STAGE CHARACTERISTICS

The compressor model equations typically depend on various stage characteristics. These stage performance characteristics are obtained experimentally at great expense and can be done only for some discrete rotational speeds. Intermediate stage characteristics have to be obtained based on some interpolation techniques. Simple polynomial surface fits have been found to be unsatisfactory for stage characteristics based on pressure coefficient and temperature coefficient versus flow coefficient. It is necessary to investigate alternate stage performance characteristics suitable for high speed compressors in order to interpolate for intermediate speeds.

4.1 CALCULATION OF STAGE CHARACTERISTICS

In lieu of the parameter flow coefficient ϕ, which is normally used, the calculation procedure proposed mainly uses two parameters, namely, total pressure loss coefficient ($\bar{\omega}$) and deviation angle (δ), represented as functions of two variables - corrected speed and angle of incidence. The deviation angle and angle of incidence are defined as shown in Fig. 23. In addition to their common use, the choice of $\bar{\omega}$ and δ is preferable to other parameters, since both are relatively insensitive to Mach numbers or corrected speeds when corrected speed is low and also not too sensitive to angle of incidence. As a test case the eight-stage axial flow compressor of the J85-13 engine has been chosen for this purpose.

In addition to $\bar{\omega}$ and δ. the procedure uses the stage temperature rise as calculated from the Euler turbine equation,

$$\frac{T_{t2}}{T_{t1}} - 1 = M_T^2 \cdot \frac{\gamma - 1}{(1 + \frac{\gamma-1}{2} M_1^2)} \left[1 - \frac{w_2}{w_1}\frac{M_1}{M_T}\cos\beta_1(\tan\beta_2' + \frac{r_1}{r_2}\frac{w_1}{w_2}\tan\beta_1)\right] \qquad (14)$$

where,

M : $\frac{V}{c}$

c: acoustic speed at station in question e.g. $M_1 = \frac{V_1}{c_1}$

M_T : $\frac{\Omega r_2}{c_1}$

M_a : $\frac{w}{c}$

w: axial velocity

N: rpm of engine, $\Omega = \frac{2\pi N}{60}$

T_t: total temperature

T: static temperature

P_t: total pressure

P_t': total pressure with respect to rotor coordinates

A = annulus area

p: static pressure

ρ = density

Subscript 0 corresponds to the variables in front of the stator, subscript 1 corresponds to the exit of stator or in front of rotor and subscript 2 is for the exit station of the rotor.

$$\beta_2' : (\beta_{2\ blade} + \delta)$$

Superscript $'$ refers to variables with respect to rotor coordinates.

The total pressure loss coefficients for stator and rotor are defined as follows.

For stator,

$$\bar{w}_s = \frac{P_{to} - P_{t1}}{P_{to} - P_o}$$

For rotor,

$$\bar{w}_r = \frac{P'_{t1} - P'_{t2}}{P'_{t1} - P_1}$$

Once the total pressure loss coefficients are available, the pressure rise can be computed in the following way. For stator,

$$\bar{w}_s = \frac{(1 - \frac{\gamma-1}{2}M_0^2)^{\frac{\gamma}{\gamma-1}} - \frac{P_1}{P_0}(1 + \frac{\gamma-1}{2}M_1^2)^{\frac{\gamma}{\gamma-1}}}{(1 + \frac{\gamma-1}{2}M_0^2)^{\frac{\gamma}{\gamma-1}} - 1} \tag{15}$$

from which P_1/P_0 can be calculated.
For rotor,

$$\bar{w}_r = \frac{(1 - \frac{\gamma-1}{2}M_1'^2)^{\frac{\gamma}{\gamma-1}} - \frac{P_2}{P_1}(1 + \frac{\gamma-1}{2}M_2'^2)^{\frac{\gamma}{\gamma-1}}}{(1 + \frac{\gamma-1}{2}M_1'^2)^{\frac{\gamma}{\gamma-1}} - 1} \tag{16}$$

from which P_2/P_1 can be calculated.

For the rotor, using the geometrical parameters. Eqs. (15) and (16) are iteratively solved along with mass balance equation, $\rho_1 w_1 A_1 = \rho_2 A_2 w_2$, in order to obtain $T_{t2}, T_2, \frac{P_2}{P_1}$ and ρ_2. This would determine the rotor exit velocity triangle completely. In the above iteration procedure T_2 is obtained from,

$$\frac{T_{t2}}{T_{t1}} = \frac{T_2(1 + \frac{\gamma-1}{2}M_2^2)}{T_1(1 + \frac{\gamma-1}{2}M_1^2)}$$

For the stator, using the geometrical parameters, Eq. (15) and mass balance equation $\rho_0 w_0 A_0 = \rho_1 w_1 A_1$ are iteratively solved to obtain $\frac{P_1}{P_0}, \rho_1$ and T_1. This would help define the stator exit velocity triangle completely. In the above iteration procedure T_1 is obtained from,

$$T_1(1 - \frac{\gamma-1}{2}M_1^2) = T_0(1 + \frac{\gamma-1}{2}M_0^2)$$

4.2 INTERPOLATION ROUTINE

The basic input curves were available for four corrected speeds, namely, 80 percent, 87 percent, 94 percent, and 100 percent. Stage characteristics were determined at all the corrected speeds using the above mentioned calculation procedure. In order to check the accuracy of the procedure, it was decided to generate the stage characteristics at 87 percent corrected speed by using the values at 80 and 94 percent corrected speeds, by means of a suitable interpolation routine. However, no noticeable pattern in the basic input curves was observed and hence linear interpolation was resorted to, between 80 and 94 percent corrected speed curves in order to generate the corresponding curves at 87 percent corrected speed. The curves thus obtained have been compared to the actual curves in Figs. 24 - 27.

4.3 RESULTS

Figures 24 and 25 show the variation of incidence angle with deviation angle for rotors 1 and 4, and correspondingly Figs. 26 and 27 show the variation of incidence angle with total pressure loss coefficient for both actual and interpolated values. In order to ascertain the effect of linear interpolation, the stage characteristics obtained using the new calculation procedure for both actual and interpolated cases, have been fed to an available code of a one-dimensional time-dependent compressor model, COMPUT and some representative values have been compared as the code reaches steady state.

Figure 28 shows the variation of inlet mass flow with time as the steady state is reached for both actual and interpolated cases and similarly the variation of outflow total temperature with time is shown in Fig. 29. As can be seen from Fig. 28 and 29, the inlet mass flow differs from the actual value by 0.61 percent and the total temperature rise across the compressor by $1.65 percent$. The last value is close to the largest deviation observed in this run.

In order to compare the method against conventional way of feeding the stage characteristics to the code (essentially, flow coefficient ϕ vs pressure coefficient ψ_p and flow coefficient ϕ vs temperature rise coefficient ψ_T), the code was fed with stage characteristics of ϕ vs ψ_p and ϕ vs ψ_T and run until the steady state is reached. Figure 30 shows the variation of inlet mass flow with time as the steady state is reached, and similarly Fig. 31 shows the variation of outflow total temperature with time. As can be seen from the results for this method, while the variation in total temperature rise remains the same as before, the variation in inlet mass flow is as much as 3.59 percent compared to the actual value.

Thus it has been noticed that in the worst case where there is no noticeable pattern in the input curves and linear interpolation is resorted to. the results are within 2 percent of the actual values by the method of stage characteristics outlined in this section. The error margin is expected to come down if the input curves are more amenable to a better interpolation routine. In any case. the current method is more suitable for high-speed compressors than using ψ_p and ψ_T vs ϕ.

5.0 MULTI-DIMENSIONAL COMPRESSOR MODELING

For studying the effects of distortion in the inlet flow and other non-uniformities in the flow field such as rotating stall on the compressor operation, one needs to consider multi-dimensional models. Kimzey and his associates (Refs. 1 and 2) generalized the one-dimensional model to account for certain three-dimensional features and yet keep the partial differential equations one-dimensional in nature. Equations representing the laws of conservation of mass, axial momentum and energy are written for each control volume. Radial and circumferential momentum fluxes are ignored. Force and shaft work terms are determined from the empirical steady-state characteristics modified for the unsteady aerodynamic response of the blades based on Goethert-Reddy analysis (Ref. 11). The radial work distribution and circumferential crossflow contribution to the swirl velocity are also accounted for, by empirical modifications to the stage characteristics. The differential equations are similar to those used in parallel compressor models. These equations are integrated in time by a Runge-Kutta method. The resulting code, while operational under some conditions, suffers from numerical instabilities under other conditions partly due to the numerical integration scheme and partly due to the method of imposing the boundary conditions.

Tesch and Steenken (Refs. 7 and 8) and Hosney and Steenken (Ref. 10) at General Electric have also considered generalizations of one-dimensional compressor models to include multi-dimensional effects for various compression systems. Tesch and Steenken have used the parallel-compressor analysis, which simulates the compressor by segmenting it circumferentially into several one-dimensional parallel compressor models. Their analysis includes circumferential total pressure and total temperature distortions and circumferential redistribution of distorted flows in blade-free volumes. The equations are solved by an explicit time-marching technique. Hosney and Steenken have developed a two-dimensional compressor model (z-r model) which allows for radial redistribution of the flow. This model is developed to account for dynamic interactions between the fan and the compressor in a turbofan compression system. For such a multi-spool system, circumferential variation of the flow is neglected and conservation equations for mass, axial and radial momentums and energy are written for a control volume in discrete form. Various forcing functions are modeled empirically through stage characteristics. Equations are integrated in time explicitly. The GE models have been applied to study the stability and frequency response of various compression systems.

Circumferentially distorted flow fields need to be studied under different operating conditions of compressors. Compressor surge and stall are intimately connected with distorted flow fields. In this section we develop the partial differential equations for a two-dimensional compressor model (z-θ model) in which flow variations in axial and circumferential directions are considered but flow variations in the radial direction are averaged out. The equations are analyzed and are transformed into compatibility equations in characteristics directions, which provide an accurate means of imposing inflow and outflow boundary conditions.

5.1 TWO-DIMENSIONAL (z-θ) COMPRESSOR MODEL EQUATIONS

We start with the Euler equations of motion for inviscid flow in conservation form in cylindrical polar coordinates. These equations are integrated in the radial direction between the hub r_1 and tip r_2. Let u, v and w be the components of velocity in the radial, circumferential and axial directions respectively. It has been assumed that the radial velocity is much smaller than the circumferential and axial velocities, i.e., $u << v, w$. Defining suitable averages of the flow field variables, the radially averaged equations of motion can be written as follows:

<u>Continuity</u>

$$\frac{\partial \bar{\rho}}{\partial t}\bar{r}L_r + \frac{\partial}{\partial z}(\overline{r\rho w}L_r) + \frac{\partial}{\partial \theta}(\overline{\rho v}L_r) + g_1 = 0 \tag{17}$$

where

$$L_r = \int_{r_1}^{r_2} dr = r_2 - r_1$$

$$\bar{r} = \frac{\int_{r_1}^{r_2} r dr}{\int_{r_1}^{r_2} dr} = \frac{1}{2}(r_1 + r_2)$$

$$\bar{\rho} = \frac{\int \rho r dr}{\int r dr}$$

$$\overline{r\rho w} = \frac{\int \rho r w dr}{\int dr}$$

$$\overline{\rho v} = \frac{\int \rho v dr}{\int dr}$$

$$g_1 = \left[r\rho u - r\rho w \frac{\partial r}{\partial z} - \rho v \frac{\partial r}{\partial \theta} \right]_{r_1}^{r_2}$$

It may be noted that while $\overline{\rho r} = \frac{\int \rho r dr}{\int dr} = \bar{\rho}\bar{r}$, in general $\overline{fg} \neq \bar{f}\bar{g}$

<u>Axial Momentum</u>

$$\frac{\partial}{\partial t}(\bar{\rho}\ \bar{w})\bar{r}L_r + \frac{\partial}{\partial z}\left[(\overline{\rho w w r} - \overline{pr})L_r \right] + \frac{\partial}{\partial \theta}(\overline{\rho v w}L_r) + g_2 = 0 \tag{18}$$

where

$$\overline{w} = \frac{\int \rho r w dr}{\int \rho r dr} = \frac{\overline{\rho r w}}{\overline{\rho r}}$$

$$\overline{\rho w w r} = \frac{\int \rho w^2 r dr}{\int dr}$$

$$\overline{\rho v w} = \frac{\int \rho v w dr}{\int dr}$$

$$\overline{p r} = \frac{\int p r dr}{\int dr}$$

$$g_2 = -\left(\overline{p}\frac{\partial r}{\partial z}\right)L_r + \left[\rho u w r - \rho v w \frac{\partial r}{\partial \theta} - (\rho w^2 + p) r \frac{\partial r}{\partial z}\right]_{r_1}^{r_2} - \overline{F}_z L_r$$

$$\overline{F}_z = \frac{\int F_z dr}{\int dr}$$

<u>Circumferential Momentum:</u>

$$\frac{\partial}{\partial t}(\bar{\rho}\bar{v})\bar{r}L_r - \frac{\partial}{\partial z}(\overline{\rho w v r}L_r) + \frac{\partial}{\partial \theta}\left[(\overline{\rho v v} + \overline{p})L_r\right] + g_3 = 0 \qquad (19)$$

where

$$\bar{v} = \frac{\int \rho r v dr}{\int \rho r dr} = \frac{\overline{\rho r v}}{\overline{\rho r}}$$

$$\overline{\rho v v} = \frac{\int \rho v^2 dr}{\int dr}$$

$$\overline{\rho w v r} = \frac{\int \rho w v r dr}{\int dr}$$

$$g_3 = \left[\rho u v r - \left(\rho v^2 + p\right)\frac{\partial r}{\partial \theta} - \rho w v r \frac{\partial r}{\partial z}\right]_{r_1}^{r_2} - \overline{F}_\theta L_r$$

$$\overline{F}_\theta = \frac{\int F_\theta dr}{\int dr}$$

Energy:

$$\frac{\partial}{\partial t}(\overline{\rho e})\bar{r}L_r + \frac{\partial}{\partial z}(\overline{\rho Hrw}\ L_r) + \frac{\partial}{\partial \theta}(\overline{\rho Hv}\ L_r) + g_4 = 0 \qquad (20)$$

where

total enthalpy, $H = e + \frac{p}{\rho}$

$$\bar{e} = \frac{\overline{\rho e r}}{\overline{\rho r}} = \frac{\int \rho e r dr}{\int \rho r dr}$$

$$\overline{\rho Hrw} = \frac{\int \rho Hrw dr}{\int dr}$$

$$\overline{\rho Hv} = \frac{\int \rho Hv dr}{\int dr}$$

$$g_4 = \left[\rho Hru - \rho Hv\frac{\partial r}{\partial \theta} - \rho Hrw\frac{\partial r}{\partial z}\right]_{r_1}^{r_2} - \overline{Q}L_r - \overline{W_s}L_r$$

$$\overline{Q} = \frac{\int Q dr}{\int dr} = \text{heat added}$$

$$\overline{W_s} = \frac{\int W_s dr}{\int dr} = \text{shaft work}$$

There are 5 equations (continuity, 2 momentum, energy and equation of state) and 15 unknowns $(\bar{r}, \bar{\rho}, \bar{w}, \bar{v}, \bar{e}, \bar{p}, \overline{r\rho w}, \overline{\rho v}, \overline{\rho w^2 r}, \overline{pr}, \overline{\rho v w}, \overline{\rho w v r}, \overline{\rho v^2}, \overline{\rho Hrw}, \overline{\rho Hv})$. $\bar{r}$ is a geometrically known quantity. Now we make an assumption that $\overline{fg} = \bar{f}\bar{g}$. This closure assumption gives 9 additional equations. Then we have 5 unknowns and 5 equations.

Among the forcing function terms $g_1, ..g_4$ in the above equations, $g_1 = 0$ if there is no mass bleed and g_2, g_3, g_4 have to be determined empirically based on suitable data correlations for stage characteristics for a particular compression system.

The above equations are of the form,

$$\frac{\partial \vec{u}}{\partial t} + \frac{\partial \vec{f_1}}{\partial z} + \frac{\partial \vec{f_2}}{\partial \theta} + \vec{g} = 0 \qquad (21)$$

where,

$$\vec{u} = \begin{pmatrix} \bar{r}L_r\bar{\rho} \\ \bar{r}L_r\bar{\rho}\bar{w} \\ \bar{r}L_r\rho v \\ \bar{r}L_r\bar{\rho}E \end{pmatrix}, \quad \vec{g} = \begin{pmatrix} g_1 \\ g_2 \\ g_3 \\ g_4 \end{pmatrix}$$

$$\vec{f}_1 = \begin{pmatrix} \overline{r\rho w}\ L_r \\ (\overline{\rho w w r} + \overline{p r})\ L_r \\ \overline{\rho w v r}\ L_r \\ \overline{\rho H r w}\ L_r \end{pmatrix} \quad \vec{f}_2 = \begin{pmatrix} \overline{\rho v}\ L_r \\ \overline{\rho v w}\ L_r \\ (\overline{\rho v v} + \overline{p})\ L_r \\ \overline{\rho H v}\ L_r \end{pmatrix}$$

These equations are hyperbolic which means that if we define the Jacobian matrices,

$$M_1 = \frac{\partial \vec{f}_1}{\partial \vec{u}}\ , \quad M_2 = \frac{\partial \vec{f}_2}{\partial \vec{u}} \tag{22}$$

The matrix $P = k_1 M_1 + k_2 M_2$, where k_1 and k_2 are arbitrary parameters such that $k_1^2 + k_2^2 = 1$, has real eigenvalues and a complete set of eigenvectors. The eigenvalues are

$$q, q, q + c \text{ and } q - c$$

where $q = k_1 v + k_2 w$, and c is the speed of sound. For axial compressor flows where the flow is primarily in the axial direction, the eigenvalues of the matrix M_1 determine the boundary condition requirements and procedures. Matrix A has eigenvalues: $w, w, w + c$ and $w - c$. For subsonic inflows this would indicate that we must prescribe three boundary conditions (equal to the number of positive eigenvalues) at the inflow boundary. We can prescribe the total pressure, total temperature and circumferential velocity or flow angle at the inlet. At the outflow boundary, if the flow is subsonic, there is one negative eigenvalue and we need to prescribe one boundary condition. This is typically the static pressure at the outflow.

Equation (21) can be integrated by a numerical scheme such as the MacCormack scheme as was done in the one-dimensional model. The boundary conditions should be imposed at the boundaries by using the characteristic compatibility equations, which can be derived by suitable transformation of Eqs. (21). These are given by

$$\frac{d\rho}{dt} - \frac{1}{c^2}\frac{d\bar{p}}{dt} + \frac{v}{r}\left(\frac{\partial \bar{\rho}}{\partial \theta} - \frac{1}{c^2}\frac{\partial \bar{p}}{\partial \theta}\right) - \frac{\bar{\rho} v}{r^2}\frac{\partial r}{\partial \theta} + \tilde{g}_1 - \frac{\tilde{g}_4}{c^2} = 0,$$

$$\text{along } \frac{dZ}{dt} = w \text{ for a fixed } \theta \tag{23}$$

$$\frac{dv}{dt} + \frac{1}{r}\left(v\frac{\partial v}{\partial \theta} + \frac{1}{\bar{\rho}}\frac{\partial \bar{p}}{\partial \theta}\right) - \frac{c^2}{\gamma r^2}\frac{\partial r}{\partial \theta} + \tilde{g}_3 = 0.$$

$$\text{along } \frac{dz}{dt} = w \text{ for a fixed } \theta \tag{24}$$

$$\frac{dw}{dt} + \frac{1}{\bar{\rho} c}\frac{d\bar{p}}{dt} + \frac{v}{r}\frac{\partial w}{\partial \theta} - \frac{c}{r}\frac{\partial c}{\partial \theta} + \frac{v}{\bar{\rho} c r}\frac{\partial \bar{p}}{\partial \theta} + \tilde{g}_2 + \frac{1}{\bar{\rho} c}\tilde{g}_4 = 0,$$

$$\text{along } \frac{dz}{dt} = w + c \text{ for a fixed } \theta \tag{25}$$

$$\frac{dw}{dt} - \frac{1}{\bar{\rho}c}\frac{d\bar{p}}{dt} + \frac{v}{r}\frac{\partial w}{\partial \theta} - \frac{c}{r}\frac{\partial v}{\partial \theta} - \frac{v}{\bar{\rho}cr}\frac{d\bar{p}}{d\theta} + \bar{g}_2 - \frac{1}{\bar{\rho}c}\bar{g}_4 = 0,$$

$$\text{along } \frac{dz}{dt} = w - c \text{ for a fixed } \theta \tag{26}$$

Details of the derivation of the eigenvalues of M_1 and the characteristic compatibility equations are outlined in Appendix A. Discretization of the equations described in this section and the corresponding Computer Code can be developed similar to the one-dimensional compressor model code COMPUT.

6.0 CONCLUSIONS

A. The numerical oscillations encountered in a one-dimensional compressor model (COMP2SP) have been traced to some parts of the algorithm. With appropriate changes, the code is now numerically stable and also it has been made more accurate by imposing the boundary conditions by the method of characteristics.

B. Numerical oscillations encountered in the turbine model (ATAC) are due to the manner in which the source functions are incorporated in the finite volume algorithm. With appropriate changes in the algorithm spurious oscillations have been eliminated in this model.

C. Stage characteristics based on the total pressure loss coefficient, $\bar{\omega}$ and the deviation angle, δ as functions of the angle of incidence, i and corrected speed have been found to be less sensitive to errors in interpolation for intermediate speeds than pressure coefficient, ψ_p and temperature coefficient, ψ_t as functions of the flow coefficient ϕ.

D. Radially averaged, unsteady two-dimensional compressor model(z-θ model) equations suitable for circumferentially distorted flows have been derived. Characteristics and compatibility equations are derived for imposing the inflow and outflow boundary conditions.

REFERENCES

1. Kimzey, W. F. "An Analysis of the Influence of Some External Disturbances of the Aerodynamic Stability of Turbine Engine Axial Flow Fans and Compressors." AEDC-TR-77-80, August 1977.

2. Chamblee, C. E., Davis, M. W. Jr., and Kimzey, W. F. "A Multistage Axial Flow Compressor Mathematical Modeling Technique with Application to Two Current Turbofan Compression Systems." AIAA-80-0054 presented at AIAA 18th Aerospace Sciences Meeting, Pasadena, CA, Jan 14-16, 1980.

3. Reddy, K. C. and Tsui, Yeng-Yung "Numerical Stability Analysis of a Compressor Model." final report of contract F40600-80-C-0006, July 1982.

4. Davis, M. W. Jr. "A Stage By Stage Compressor Modeling Technique for Single and Dual Spool Compression System." a thesis presented for Master of Science degree to The University of Tennessee, August 1981.

5. "Aerodynamic Design of Axial Flow Compressors." NASA SP 36, 1965.

6. Kerrebrock, T. L. *Aircraft Engines and Gas Turbines.* MIT Press, 1977.

7. Tesch, W. A. and Steenken, W. G. "Blade Row Dynamic Digital Compressor Program, Vol. I J85 Clean Inlet Flow and Parallel Compressor Models." NASA CR-134978. March 1976.

8. Tesch, W. A. and Steenken, W. G. "Blade Row Dynamic Digital Compressor Program, Vol. II J85 Circumferential Distortion Redistribution Model. Effect of Stator Characteristics and Stage Characteristics Sensitivity Study." NASA CR-134953, July 1978.

9. Kimzey, W. F. "An Analysis of the Influence of Some External Disturbances on the Aerodynamic Stability of Turbine Engine Axial Flow Fans and Compressors." A dissertation presented for the degree of Doctor of Philosophy to University of Tennessee. June 1977.

10. Hosney, W. M., and Steenken. W. G. "TF34 Engine Compression System Computer Study." NASA CR-159889, June 1979.

11. Goethert, B. H., and Reddy. K. C. "Unsteady Aerodynamics of Rotor Blades of a Compressor Under Distorted Flow Conditions." Paper presented at AGARD Fluid Dynamics Panel Specialist Meeting on Aerodynamic Interference, Silver Springs, Maryland. September 28-30, 1970.

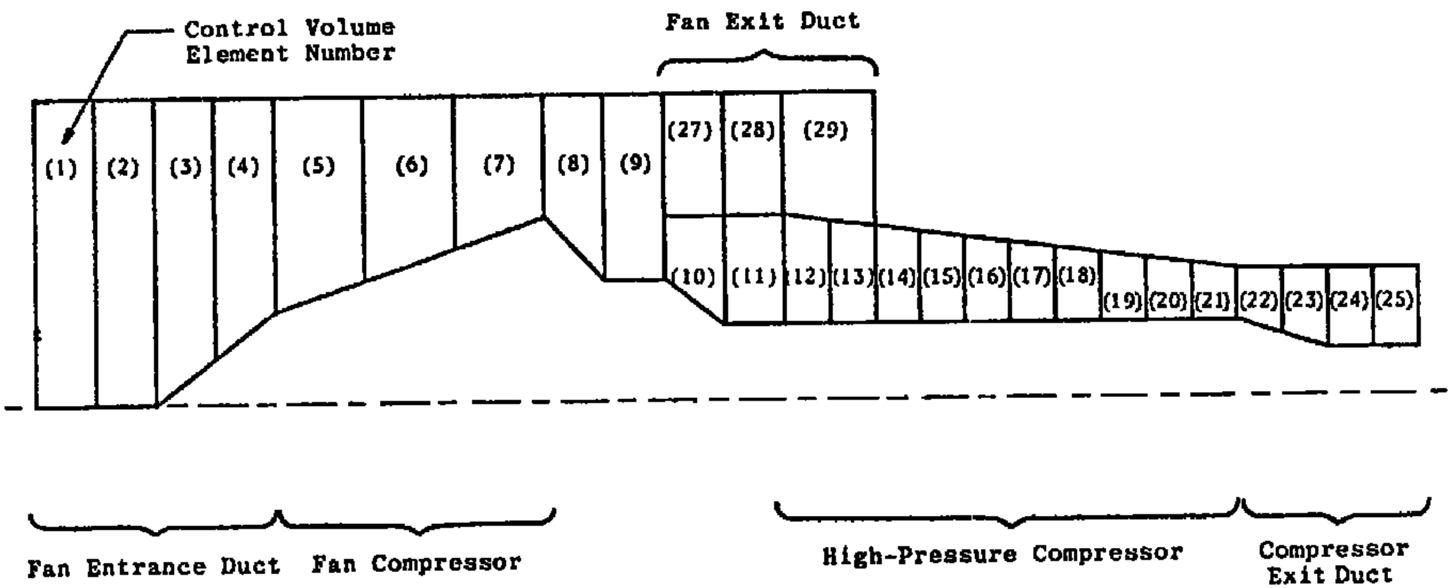

Figure 1. Schematic of the 13-stage, dual-spool compression system model.

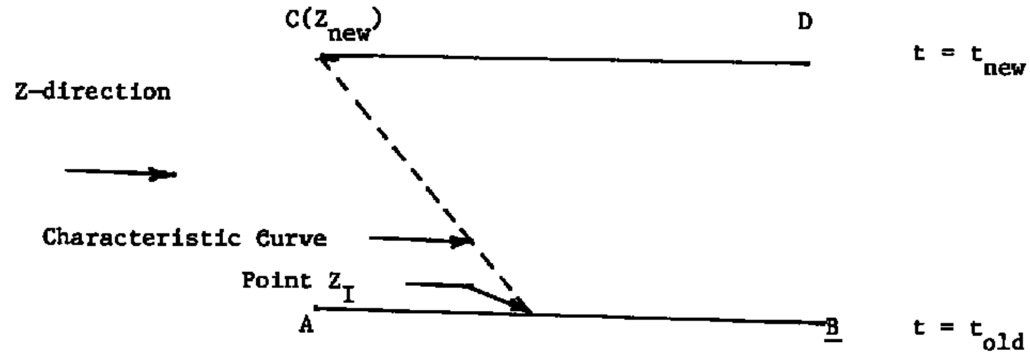

Figure 2. Schematic of inlet characteristic boundary scheme.

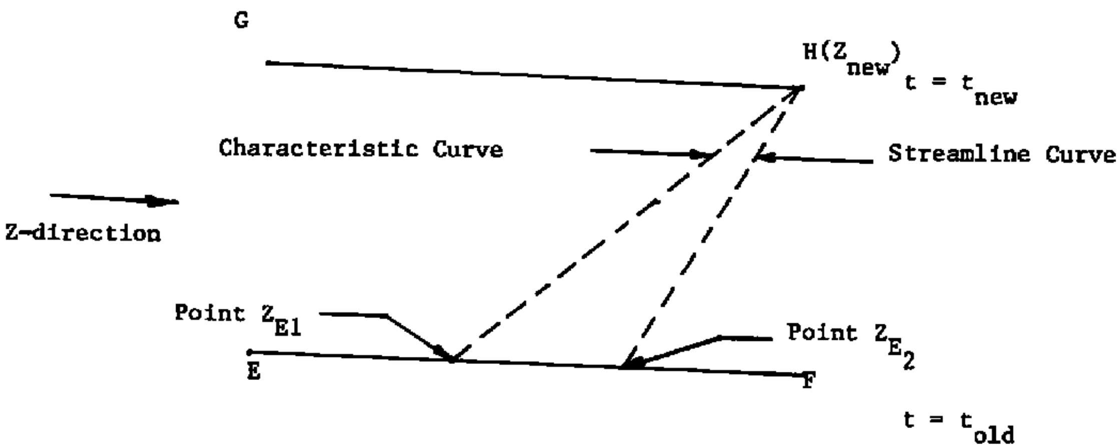

Figure 3. Schematic of exit characteristic boundary scheme.

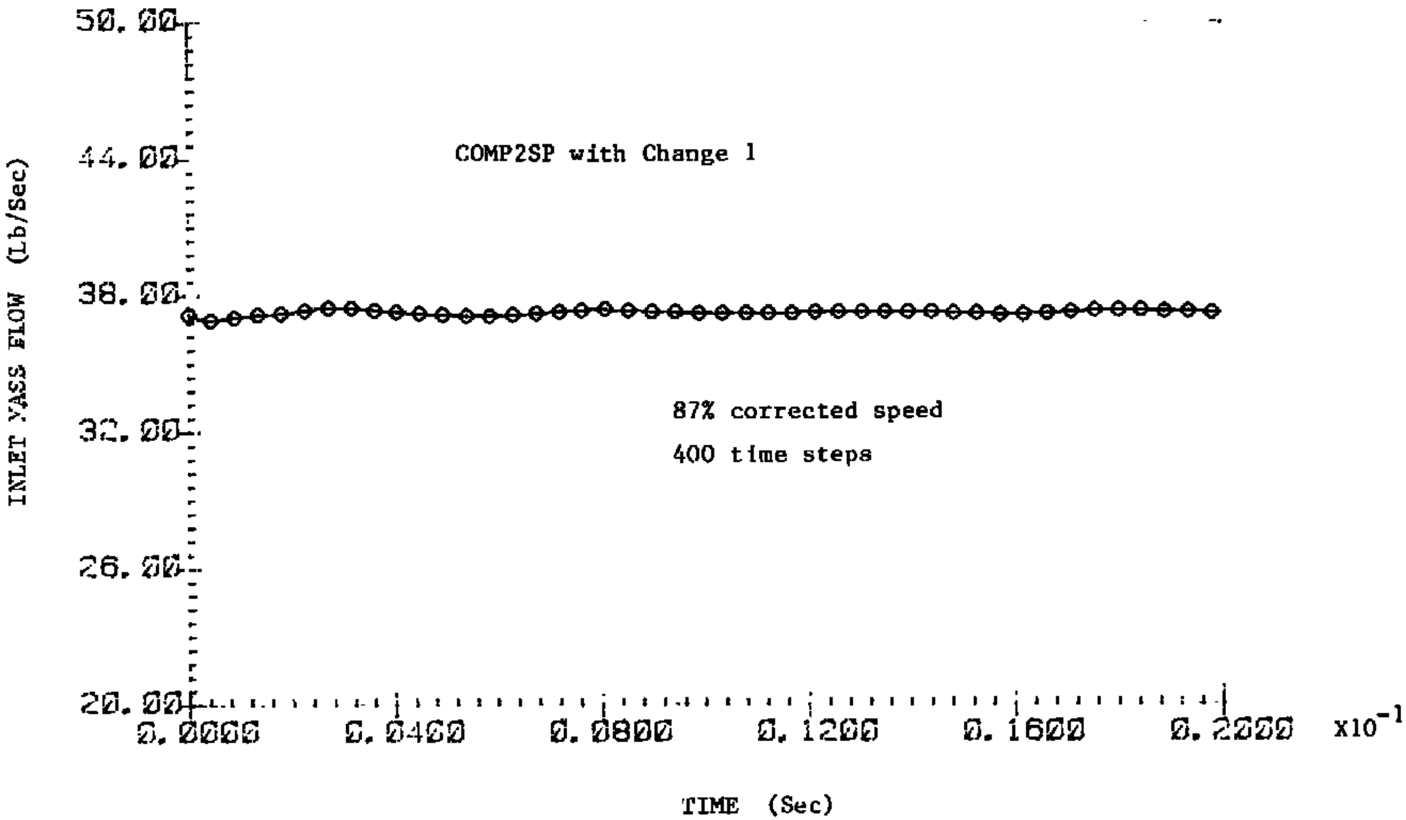

Figure 4. Inlet mass flow versus time with change 1 (COMP2SP).

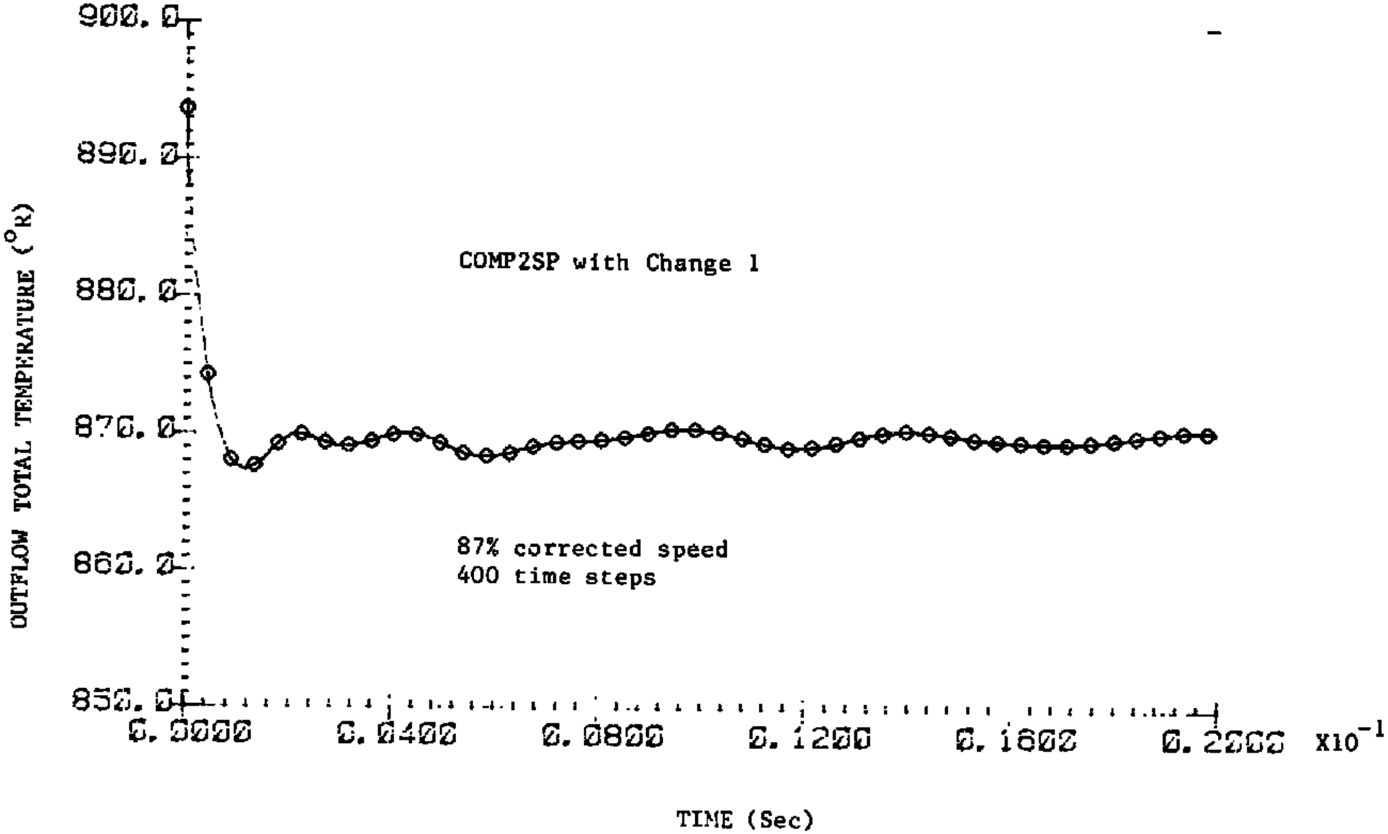

Figure 5. Outflow total temperature versus time with change 1 (COMP2SP).

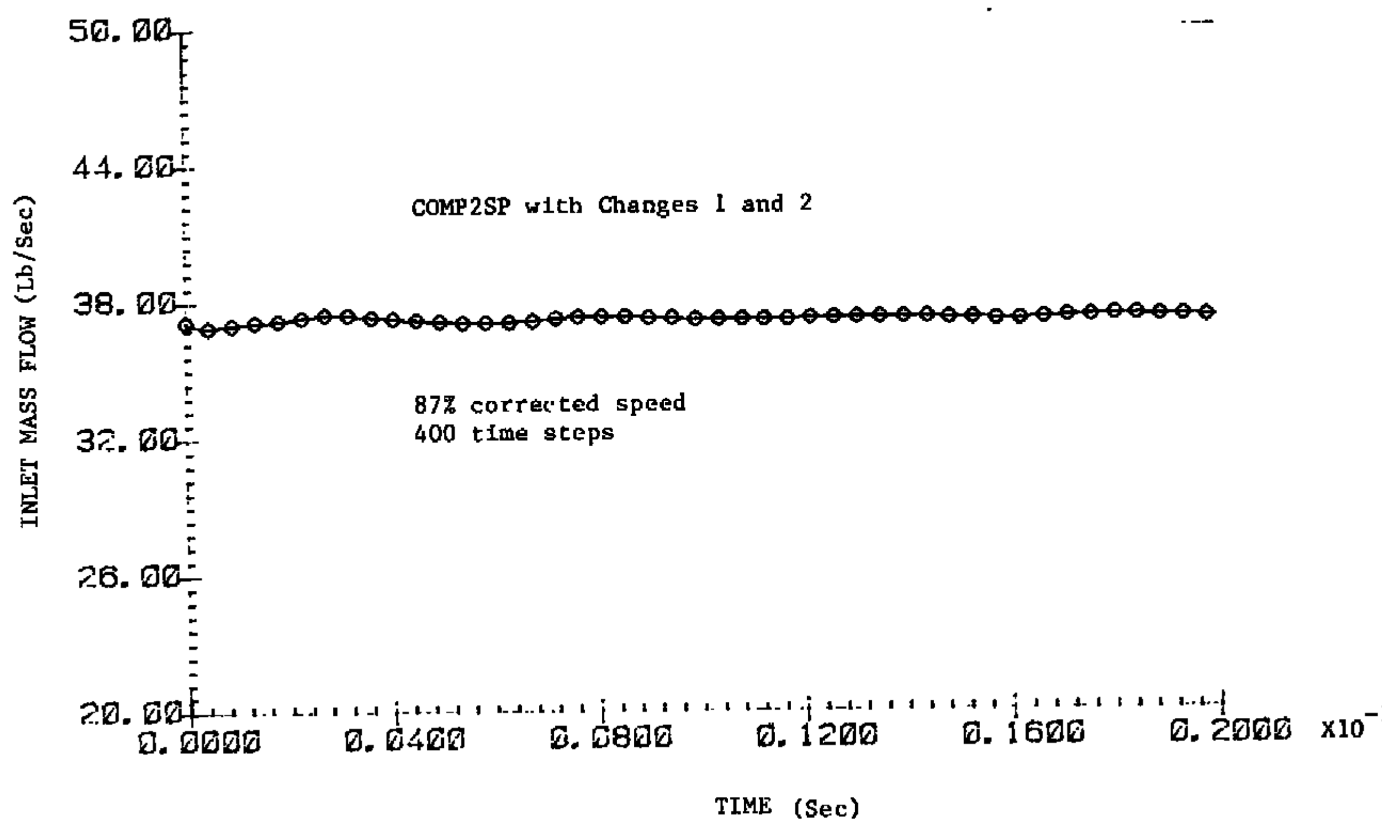

Figure 6. Inlet mass flow versus time with changes 1 and 2 (COMP2SP).

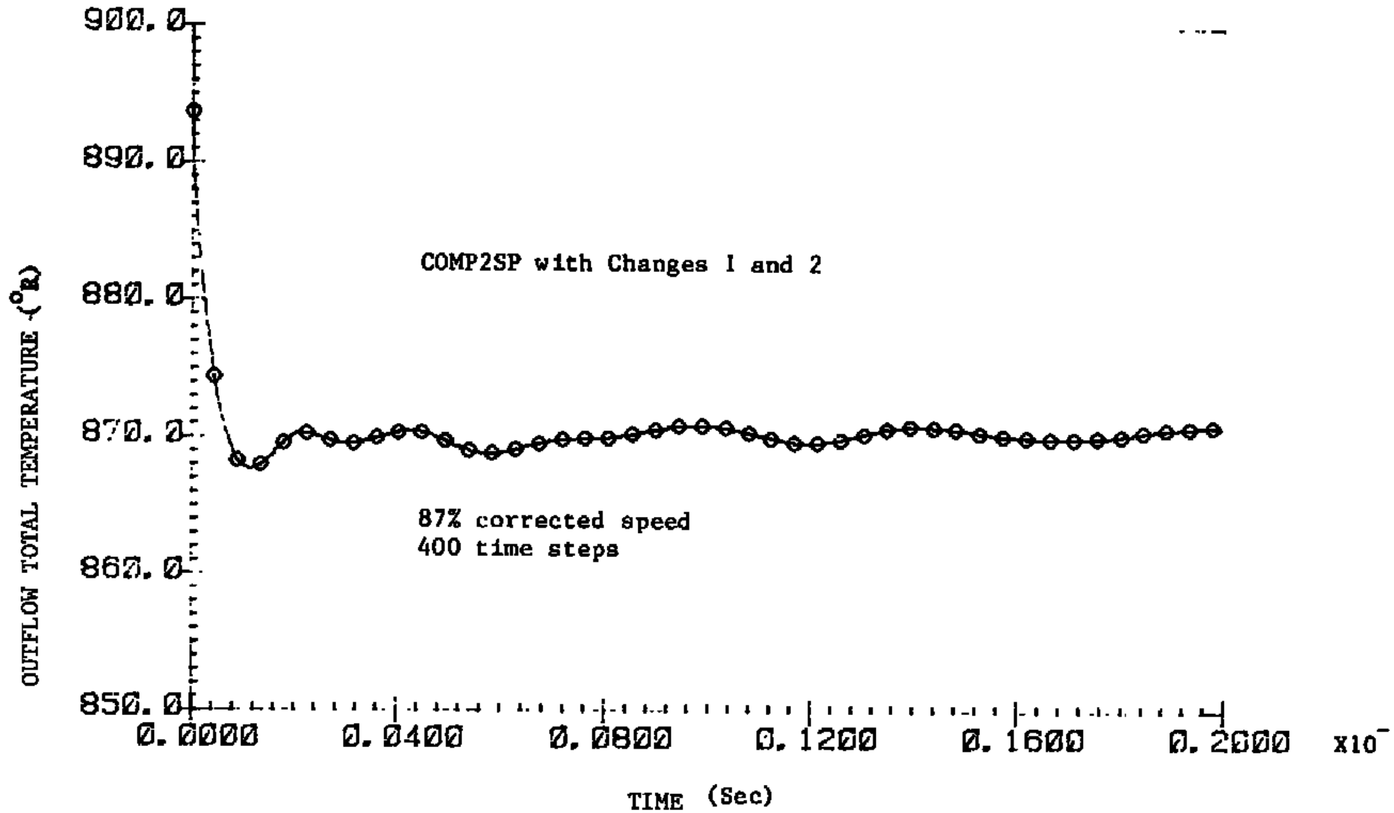

Figure 7. Outlfow total temperature versus time with changes 1 and 2 (COMP2SP).

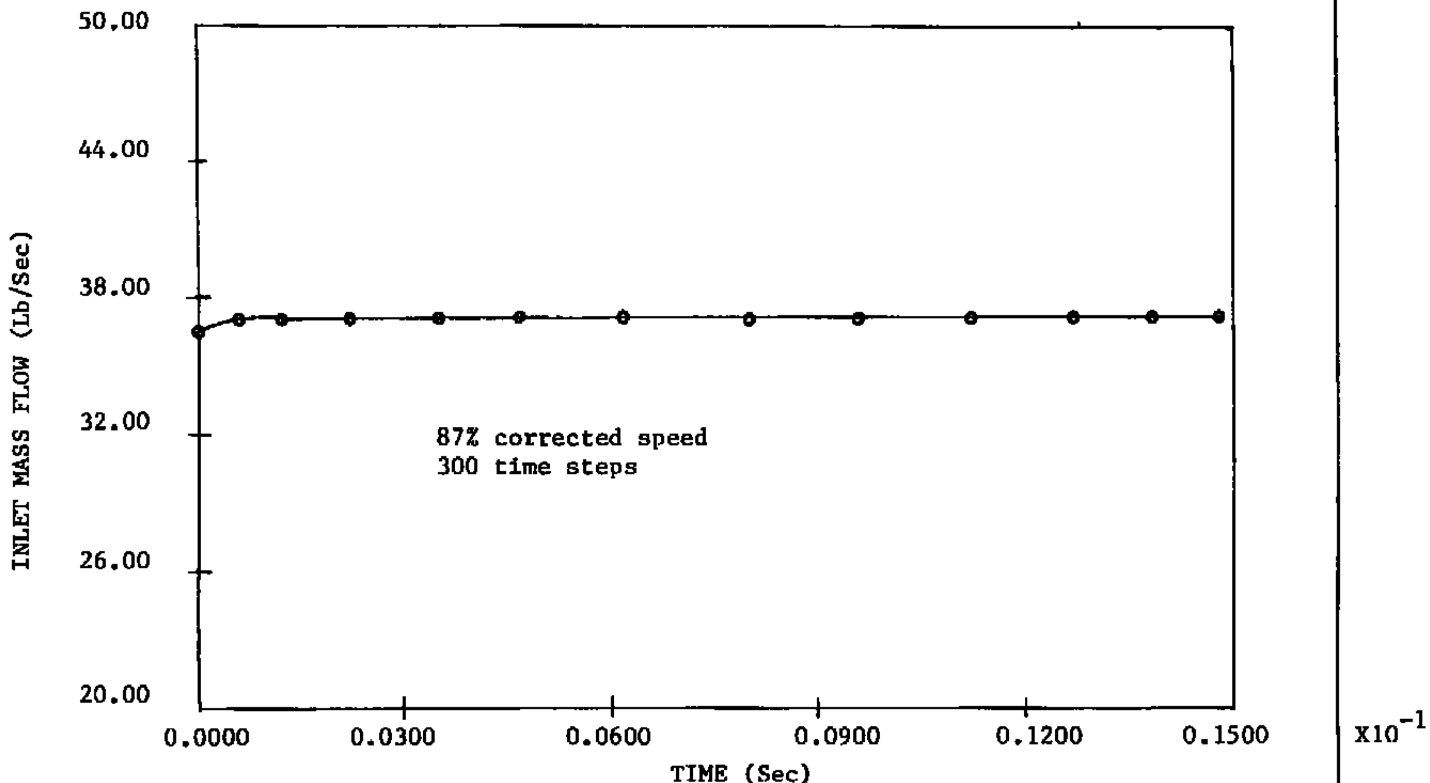

Figure 8. Inlet mass flow versus time with changes 1, 2, and 3 (COMP2SP).

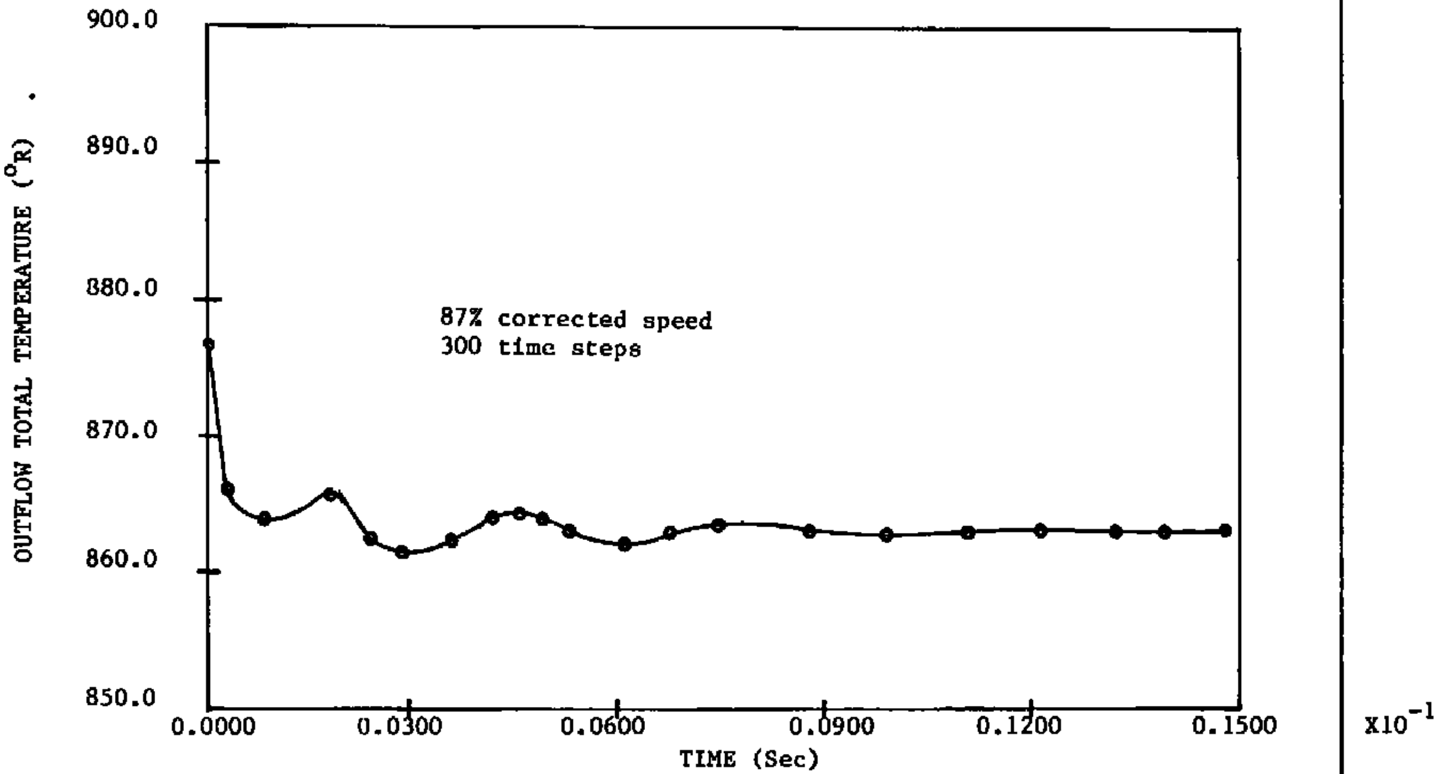

Figure 9. Outflow total temperature versus time with changes 1, 2, and 3 (COMP2SP).

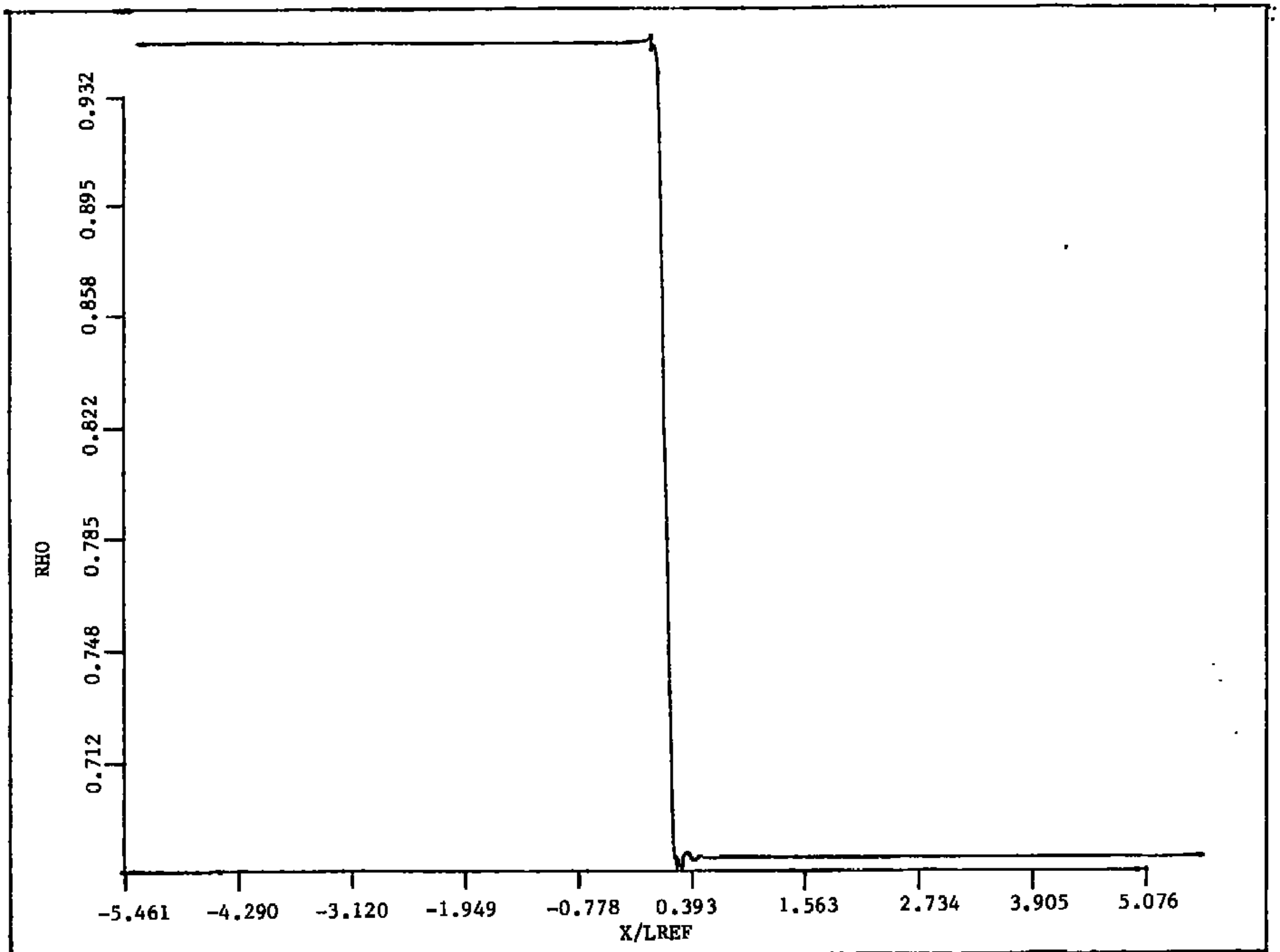

Figure 10. Steady-state distribution of density with oscillations (4,800 time steps).

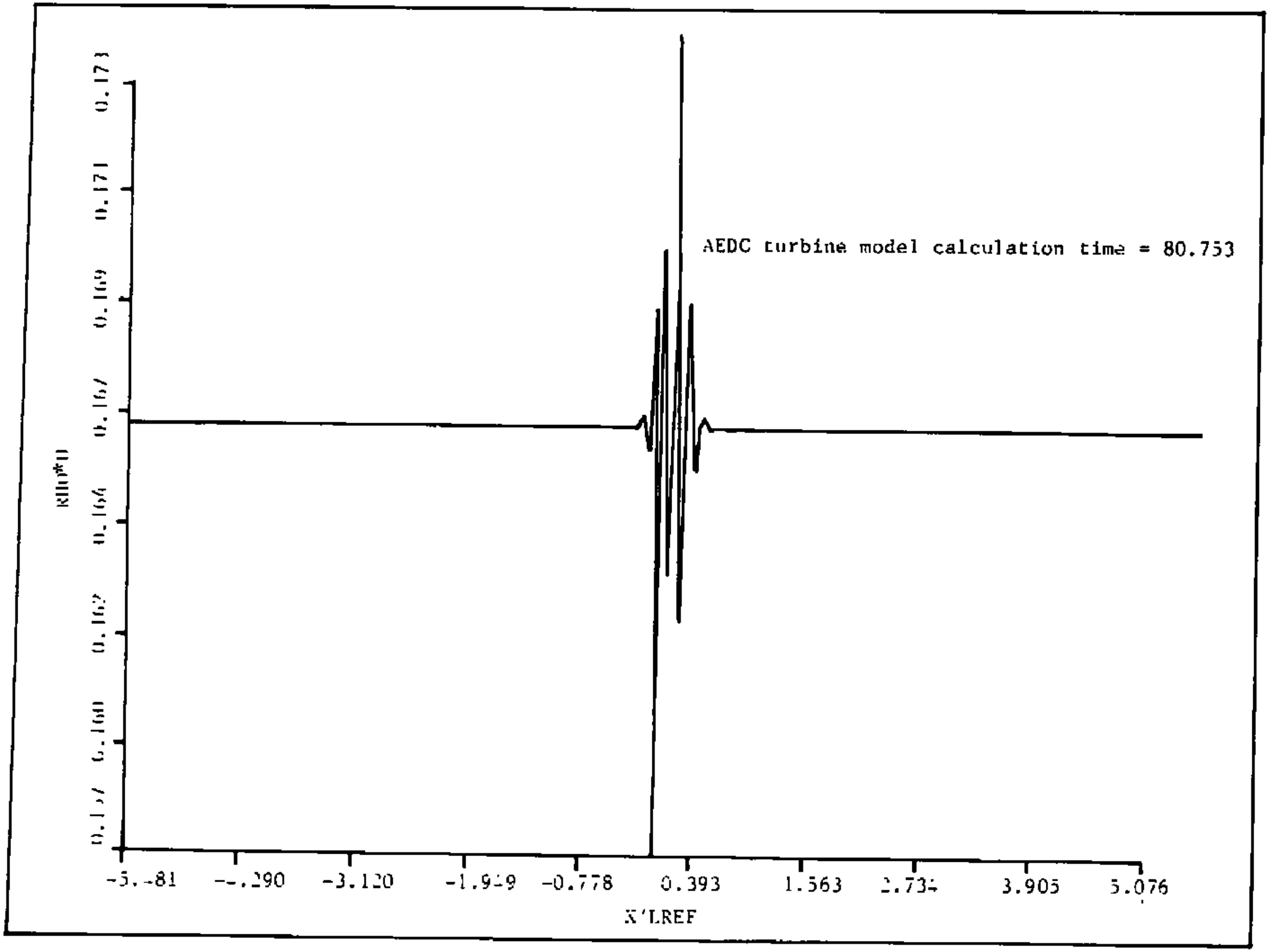

Figure 11. Steady-state distribution of mass flux with oscillations (4,800 time steps).

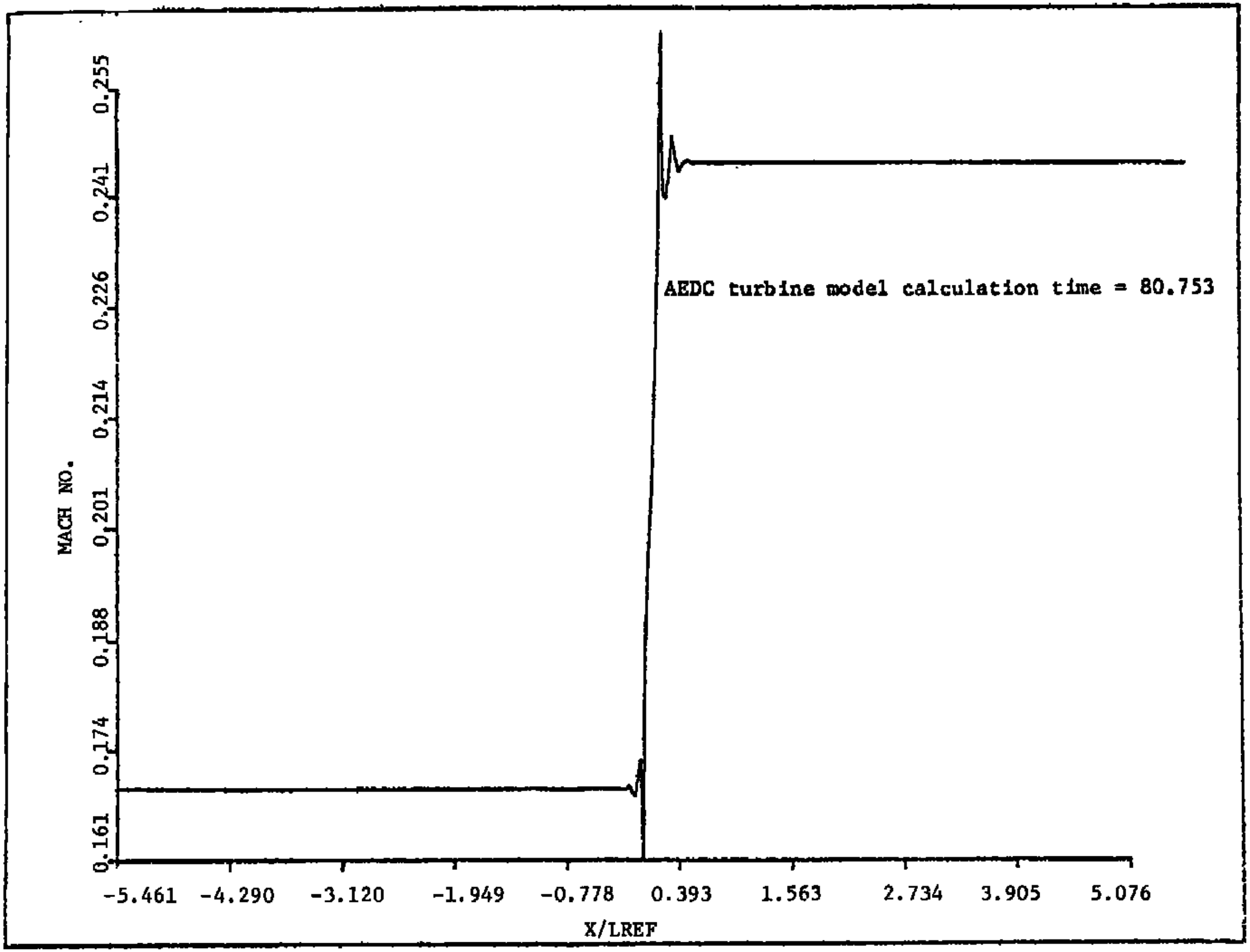

Figure 12. Steady-state distribution of Mach number with oscillations (4,800 time steps).

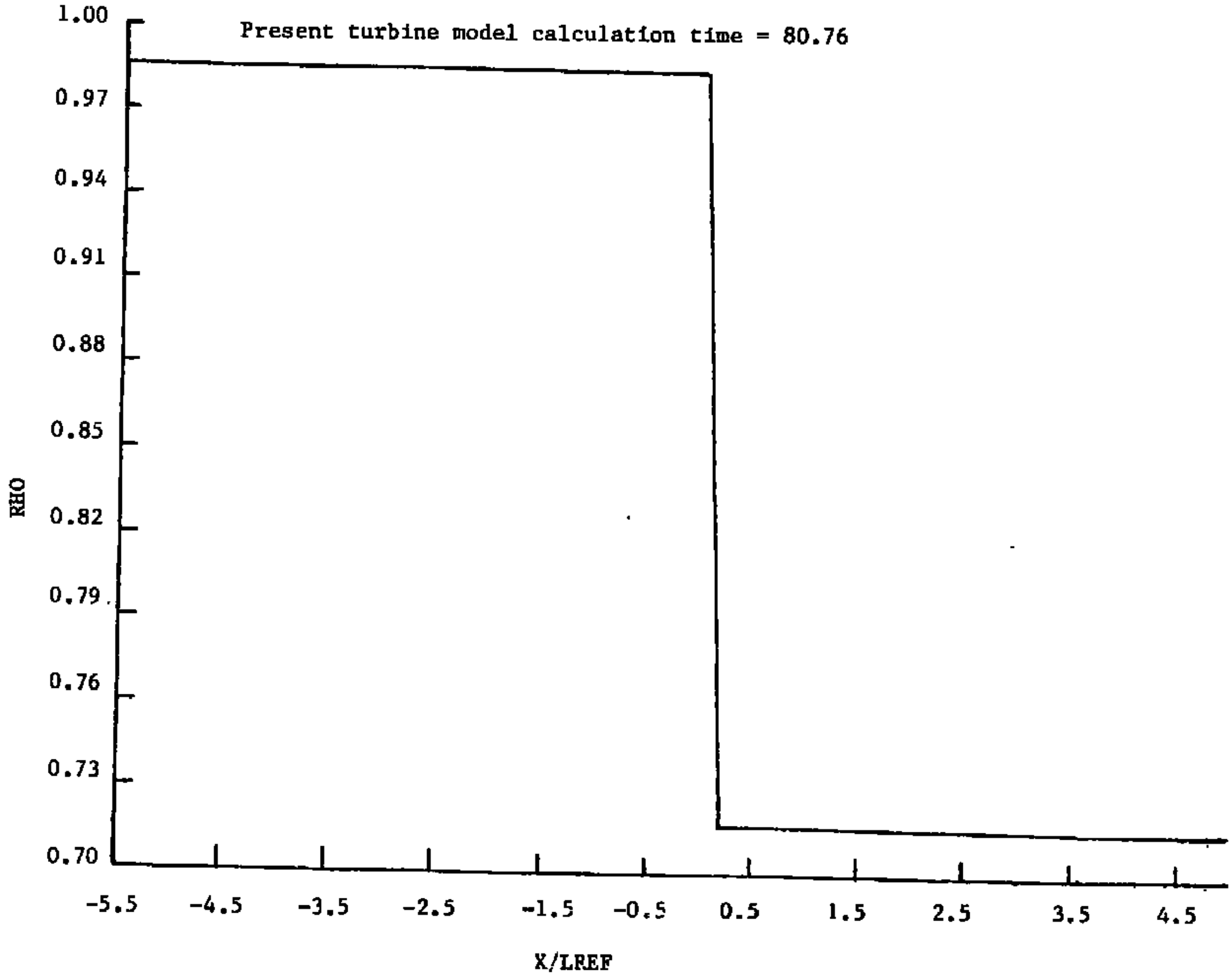

Figure 13. Steady-state distribution of density (TURBUT).

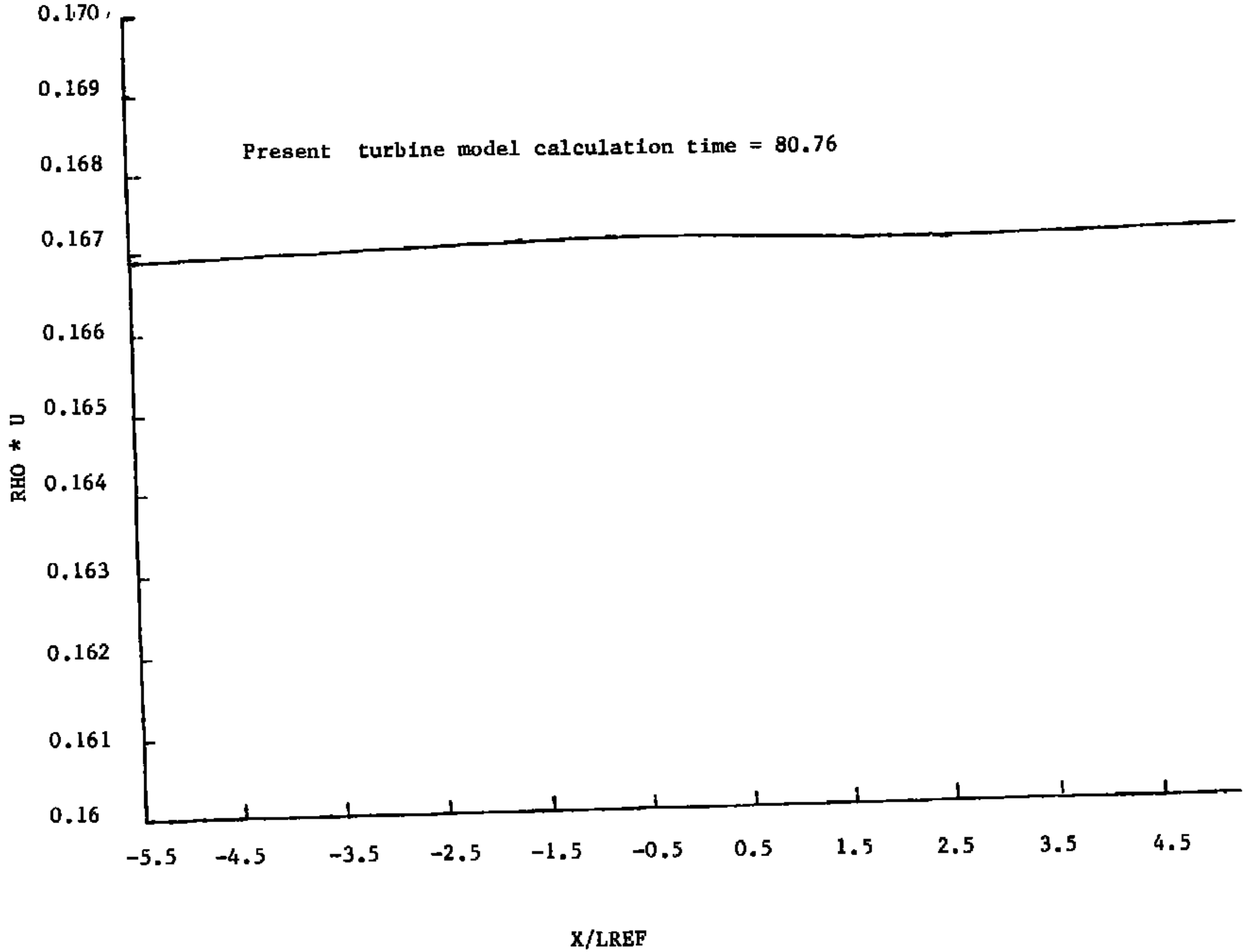

Figure 14. Steady-state distribution of mass flux (TURBUT).

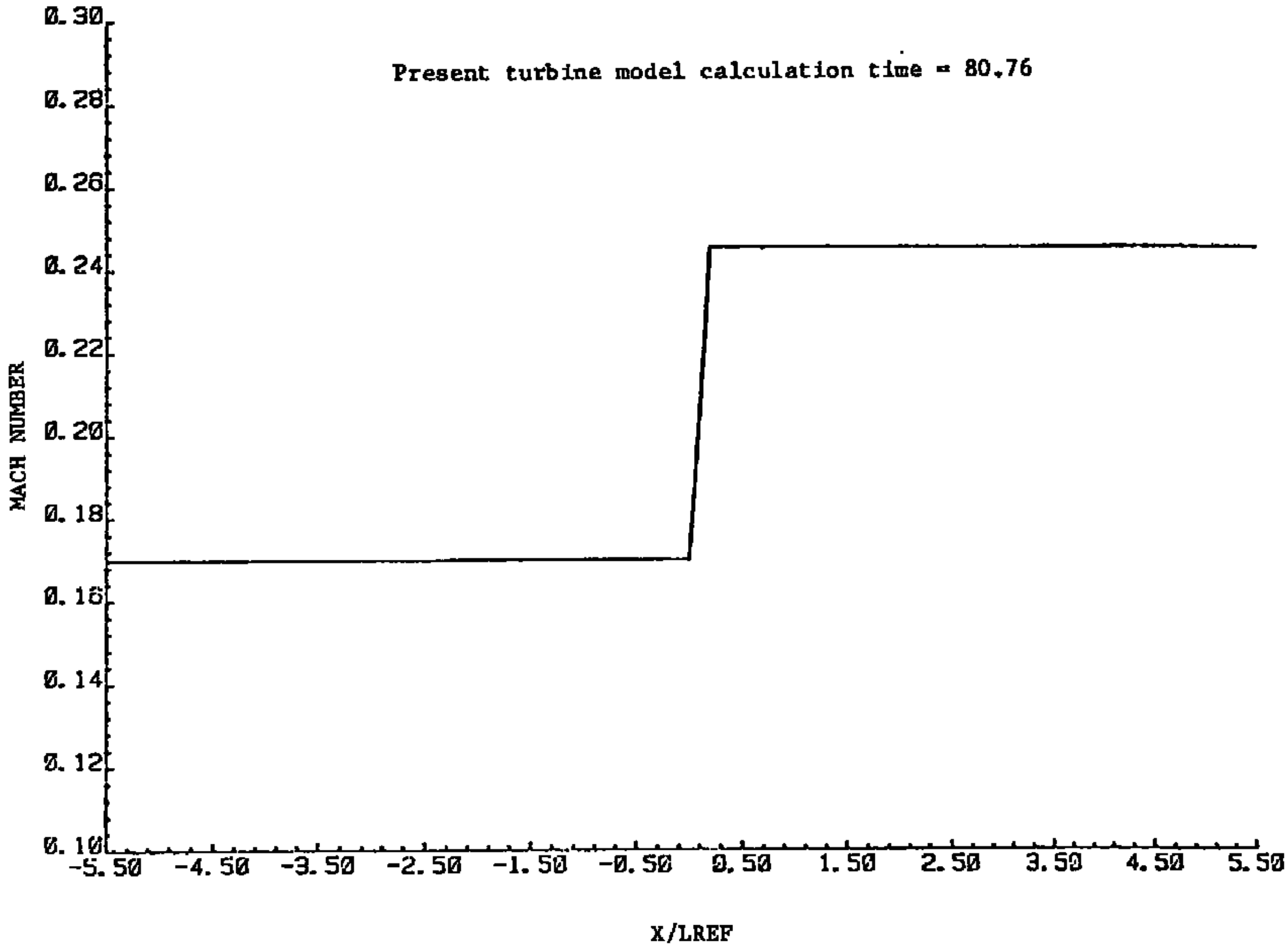

Figure 15. Steady-state distribution of Mach number (TURBUT).

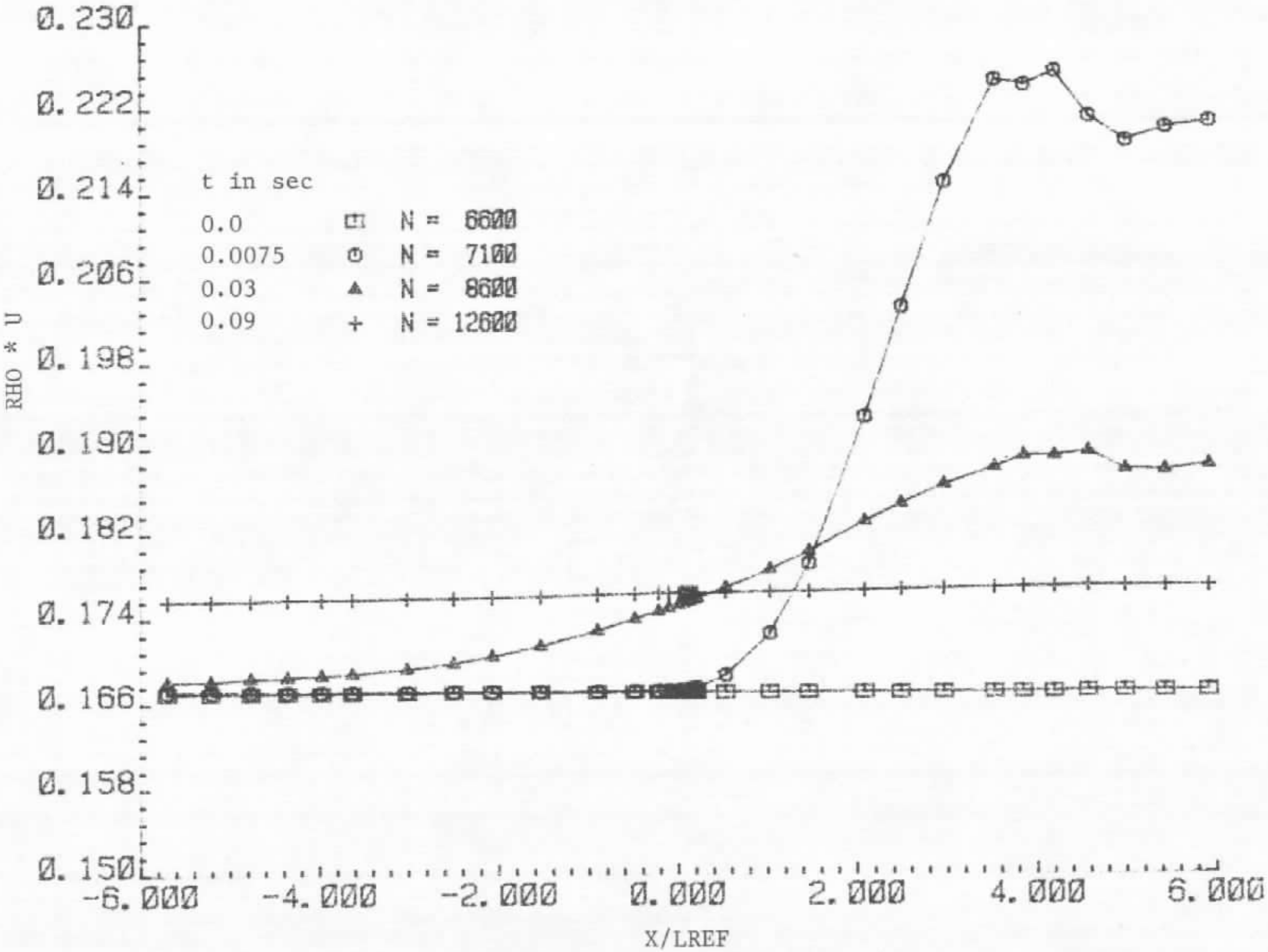

Figure 16. Evolution of mass flow from one steady-state condition to another as exit pressure is dropped impulsively from 9.485 psi to 8 psi at t = 0.0.

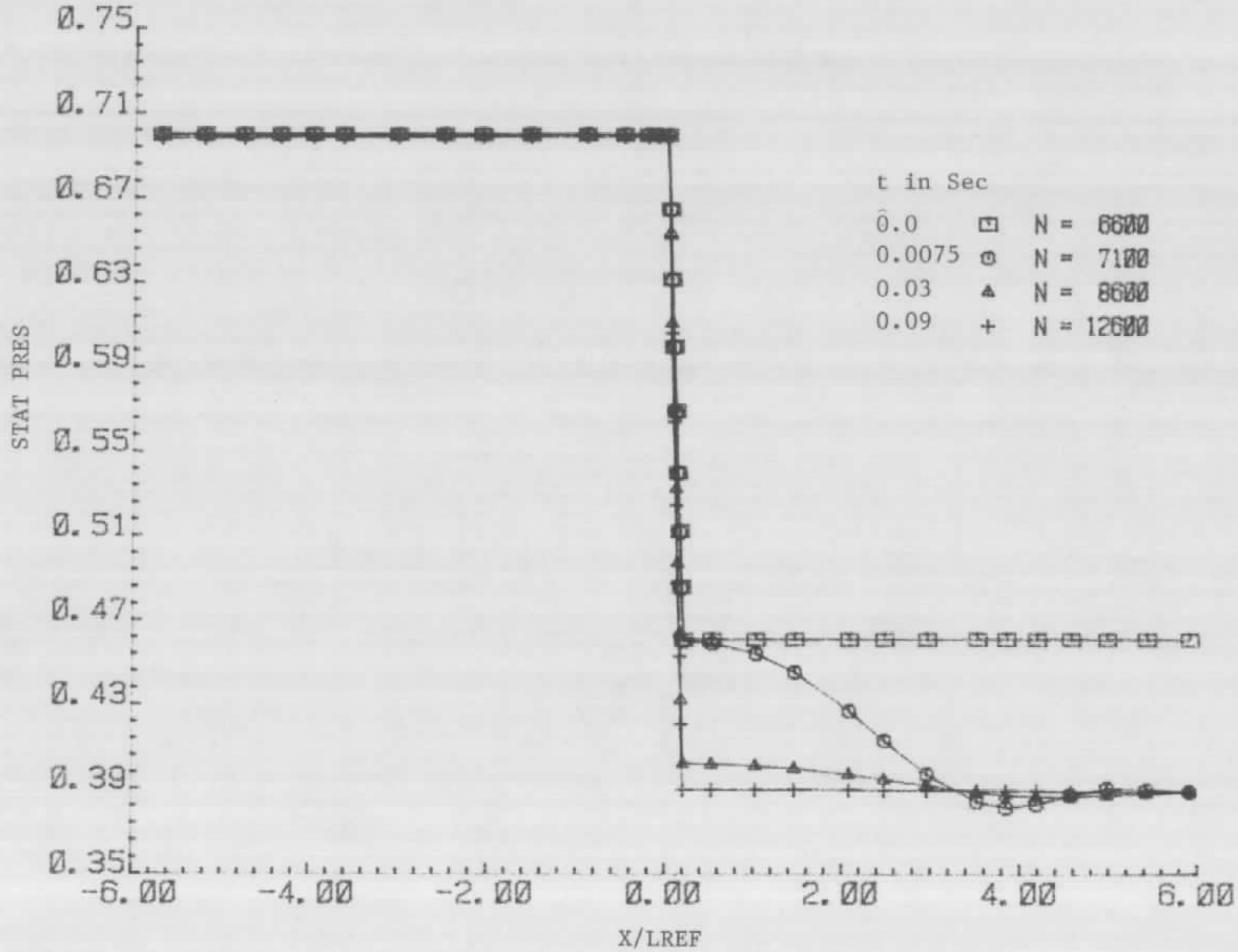

Figure 17. Evolution of static pressure from one steady-state condition to another as exit pressure is dropped impulsively from 9.485 psi to 8 psi at t = 0.0.

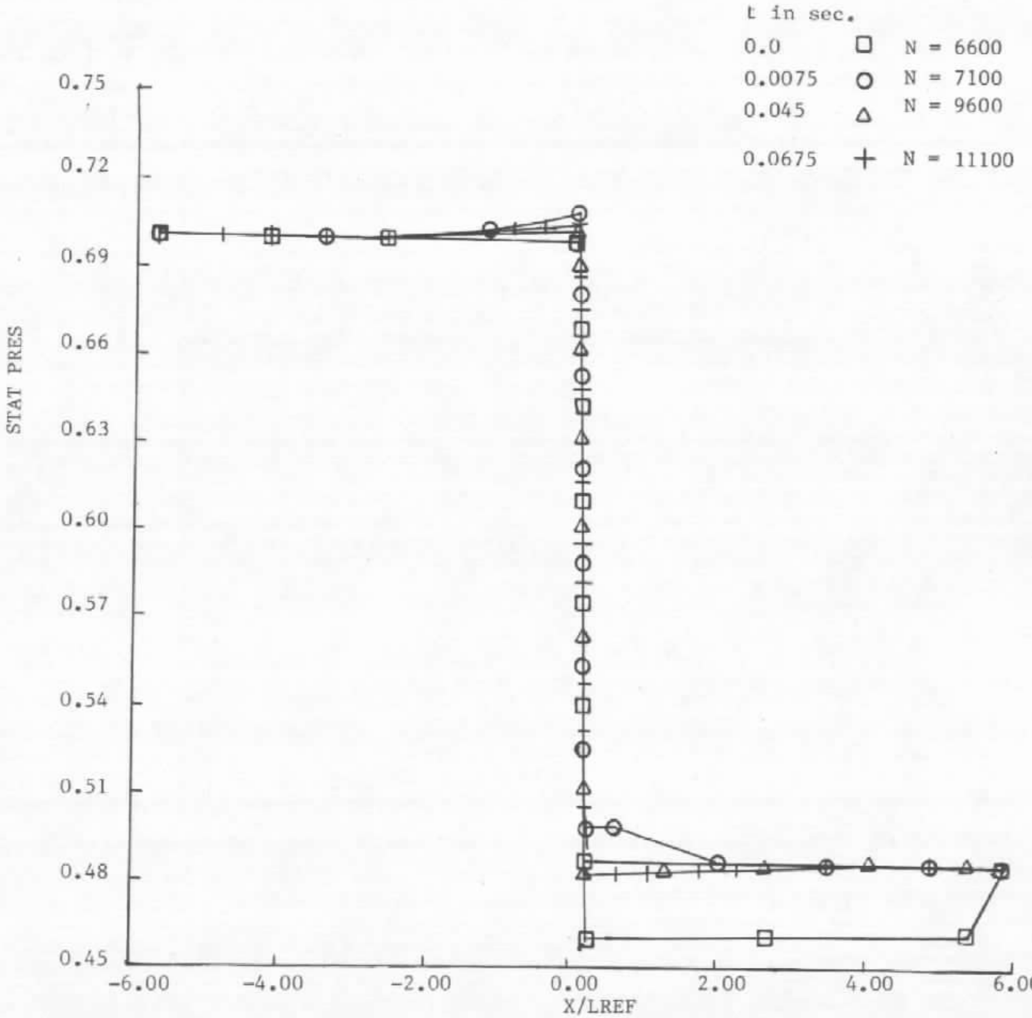

Figure 18. Evolution of static pressure from one steady-state condition to another as the exit pressure is increased impulsively from 9.485 to 10 psi at t = 0.0.

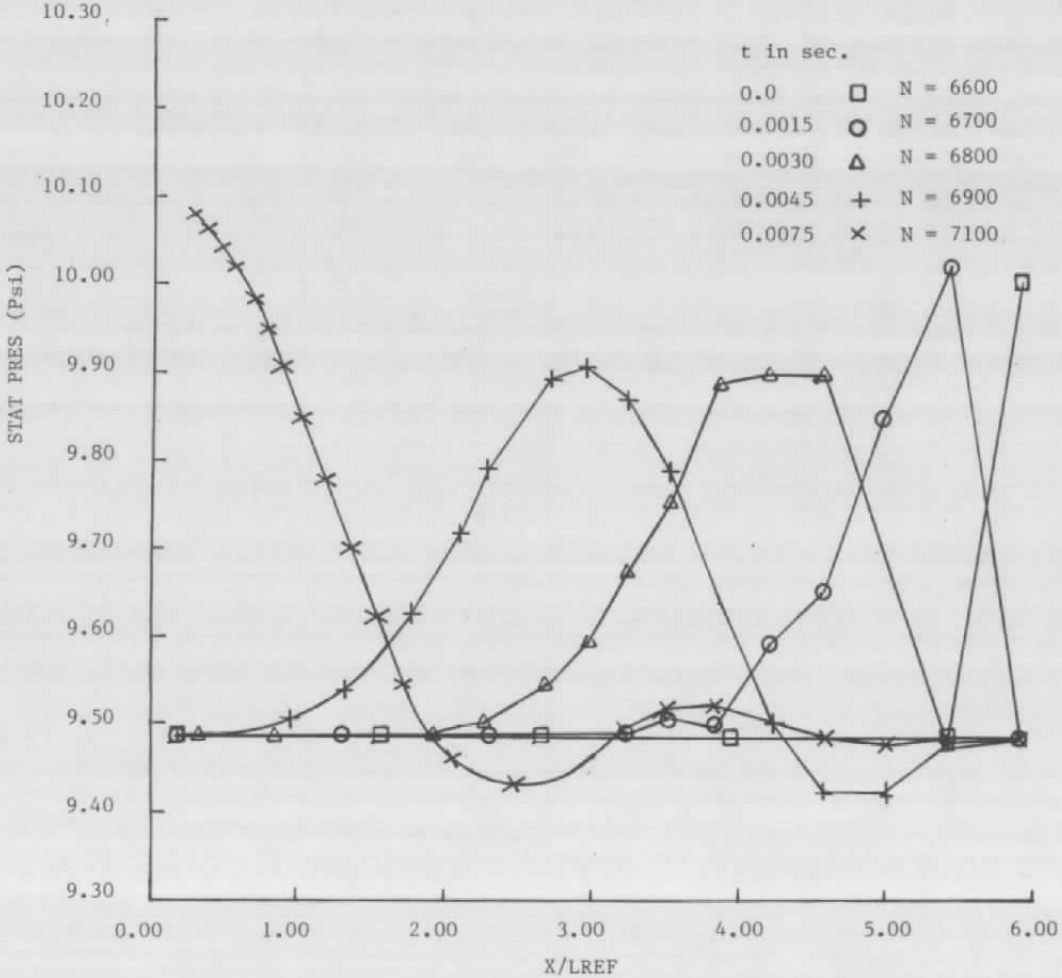

Figure 19. Upstream propagation of a pressure pulse in the downstream side duct of a turbine.

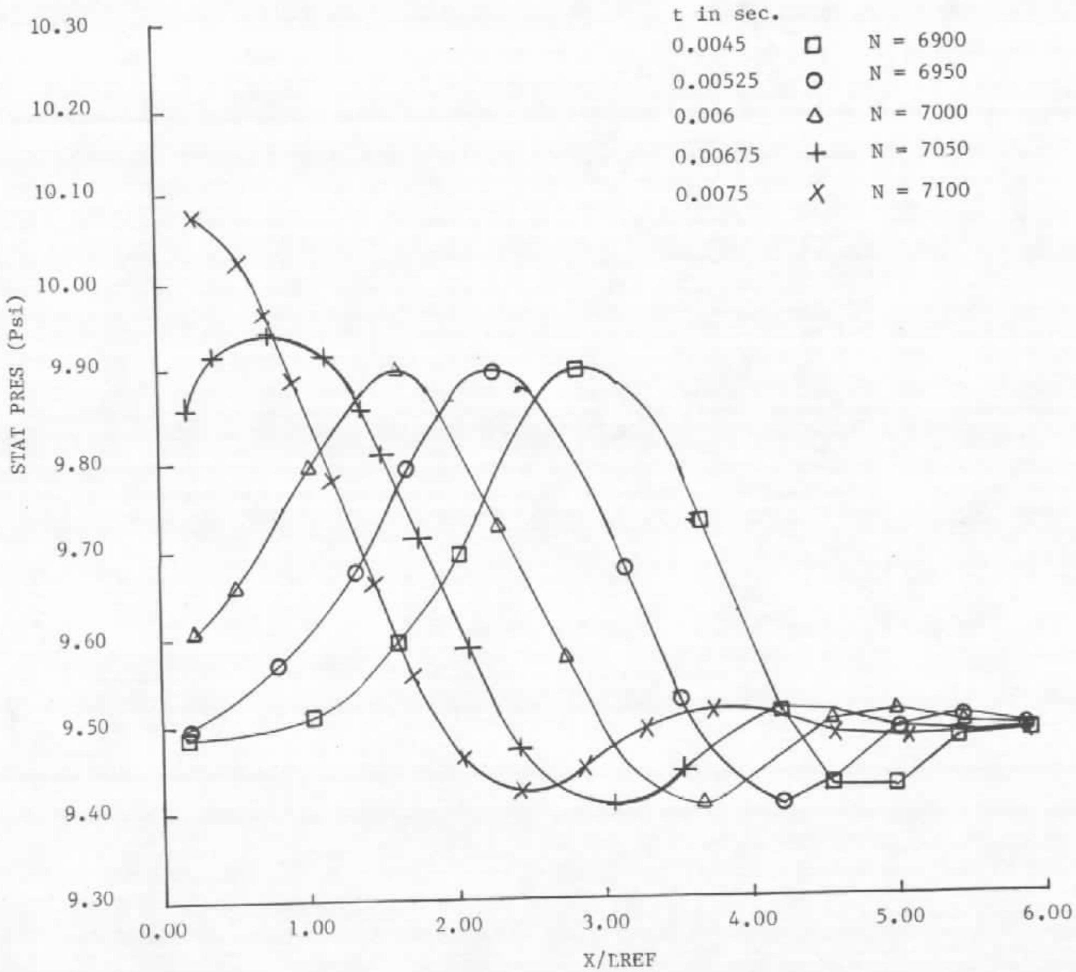

Figure 20. Upstream propagation of a pressure pulse in the downstream side duct of a turbine.

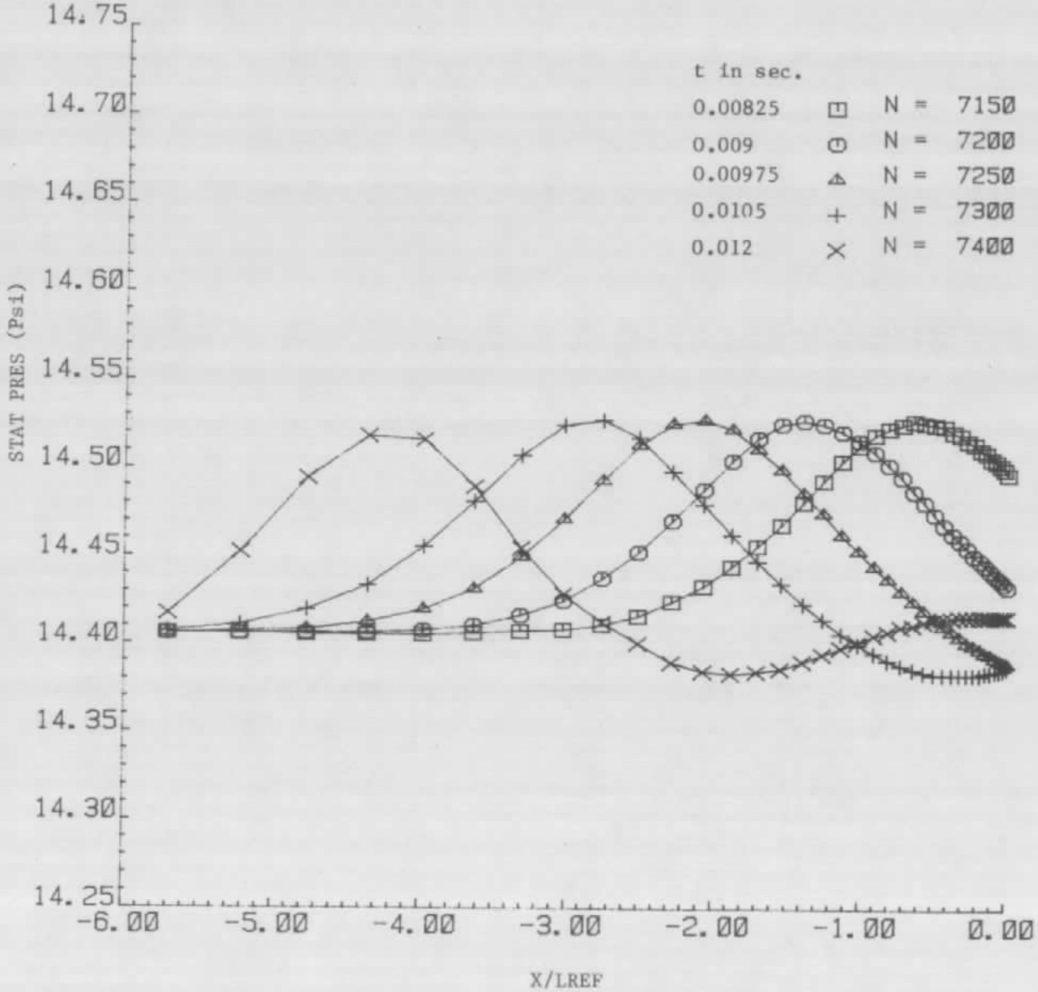

Figure 21. Upstream propagation of a pressure pulse in the upstream side duct of a turbine.

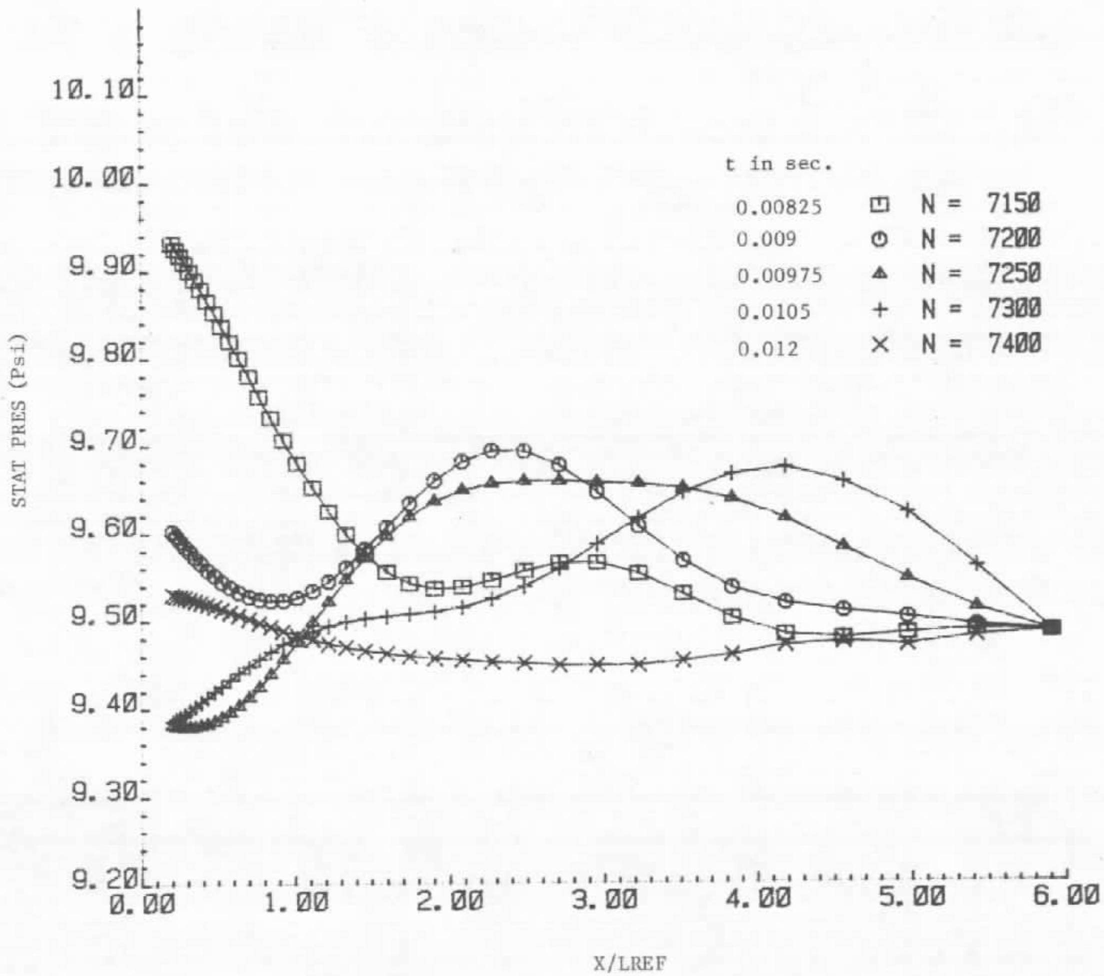

Figure 22. Interaction of the pressure pulse with reflections from the turbine and the downstream duct exit.

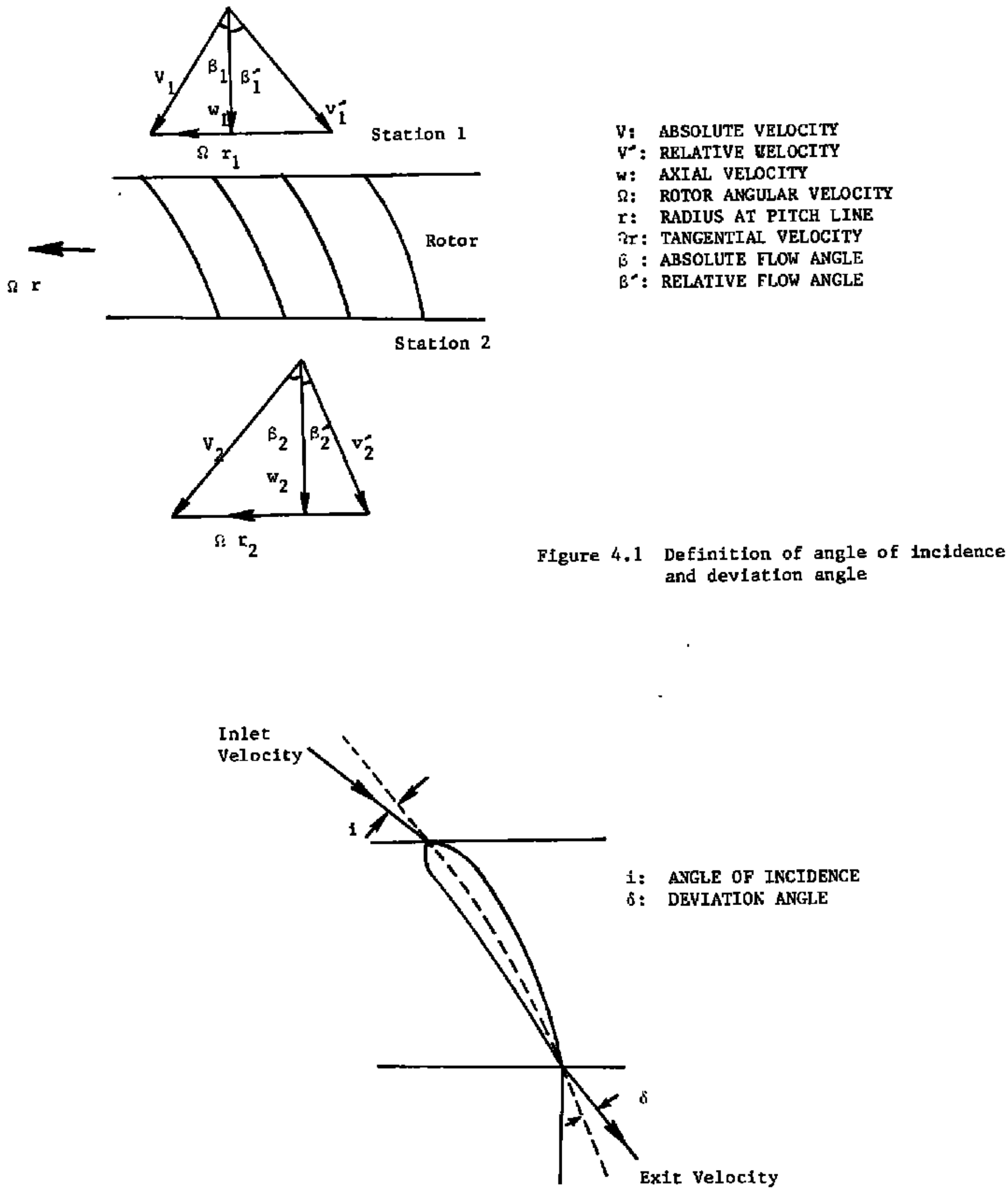

Figure 23. Definition of angle of incidence and deviation angle.

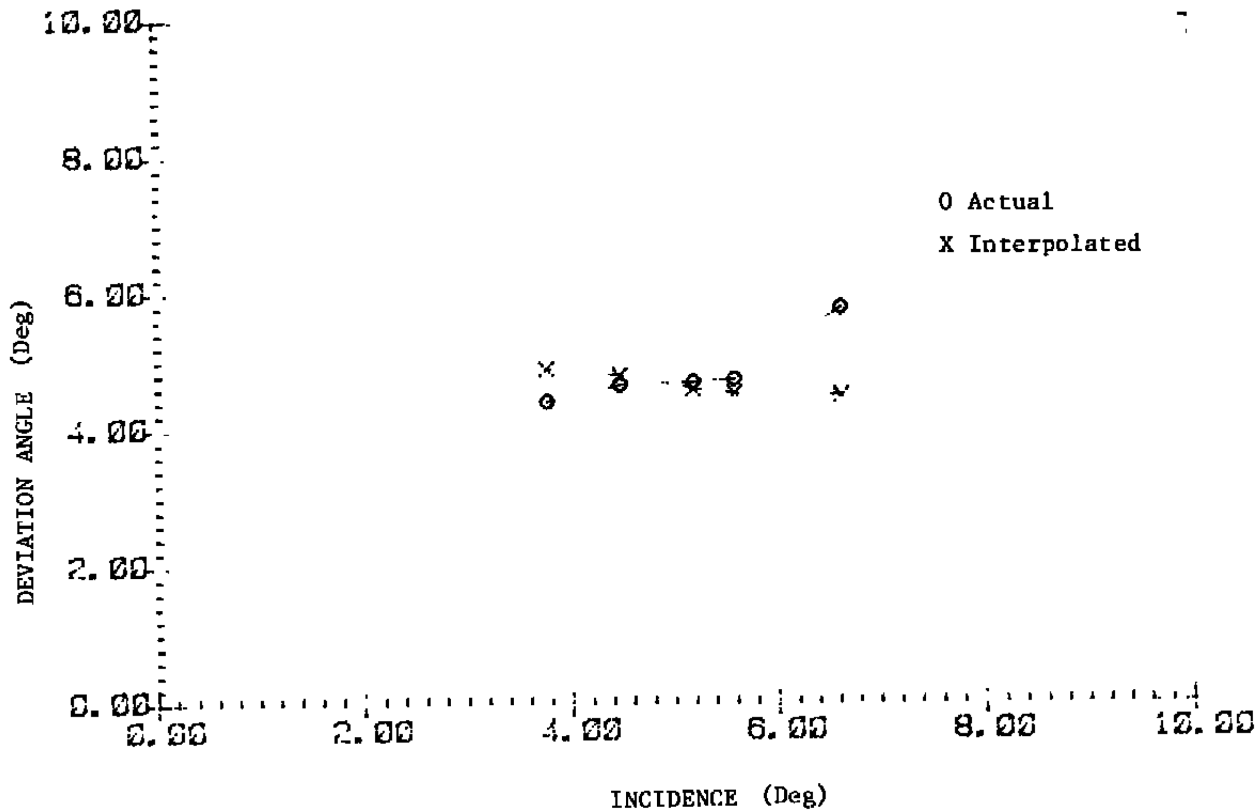

Figure 24. Actual and interpolated curves of deviation angle versus angle of incidence (Rotor 1).

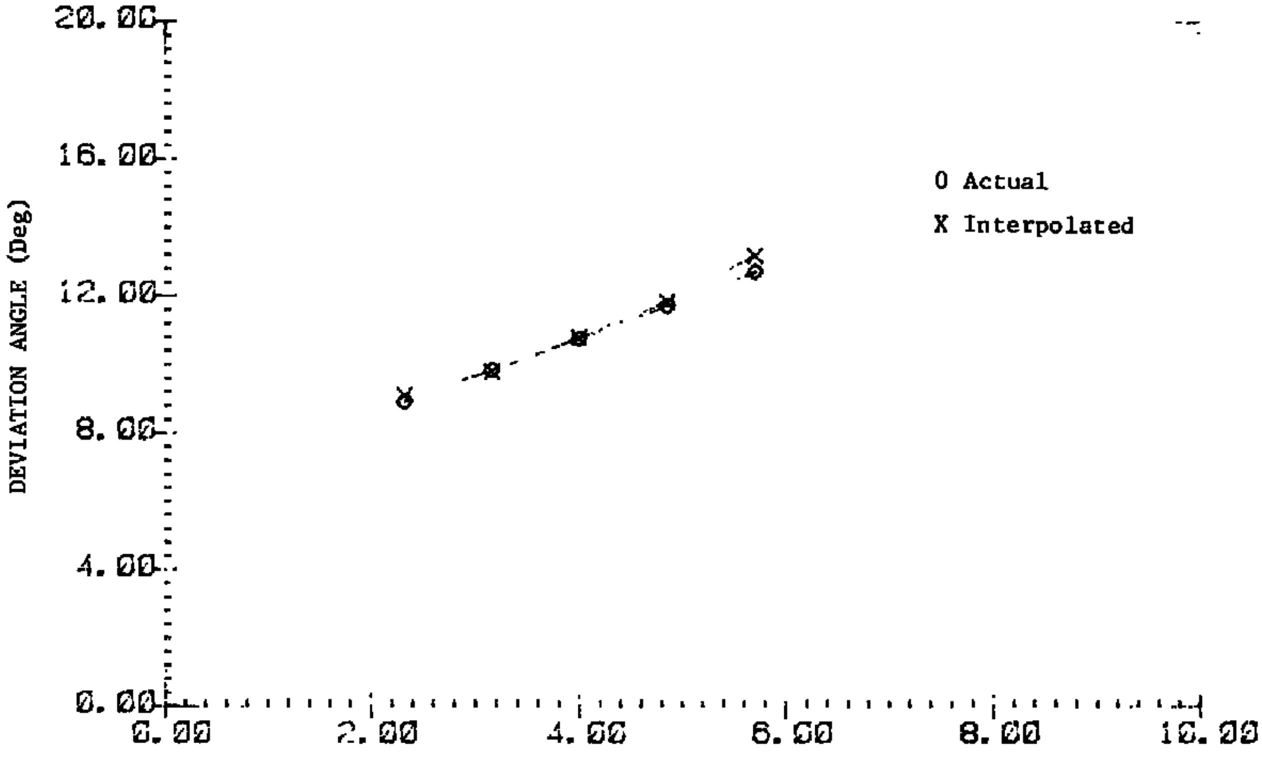

Figure 25. Actual and interpolated curves of deviation angle versus angle of incidence (Rotor 4).

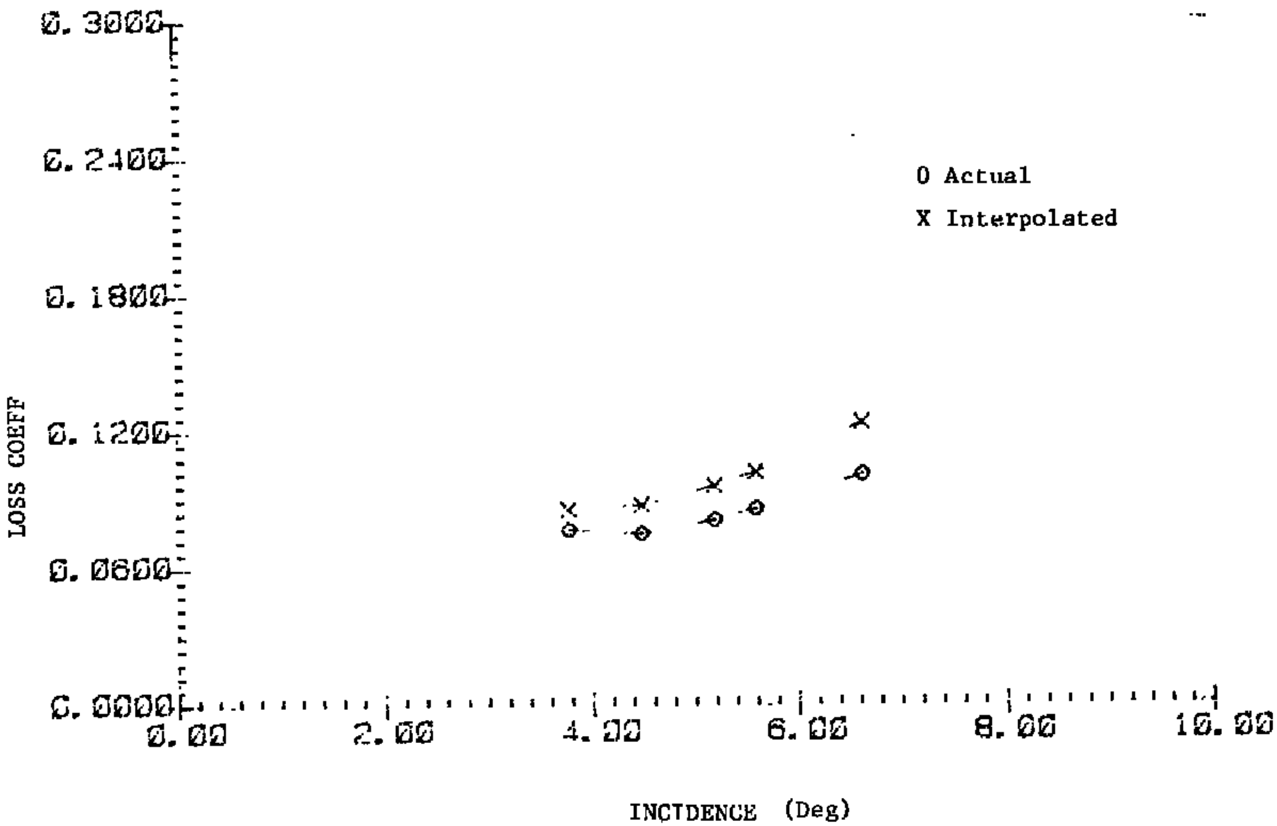

Figure 26. Actual and interpolated curves of total pressure loss coefficient versus angle of incidence (Rotor 1).

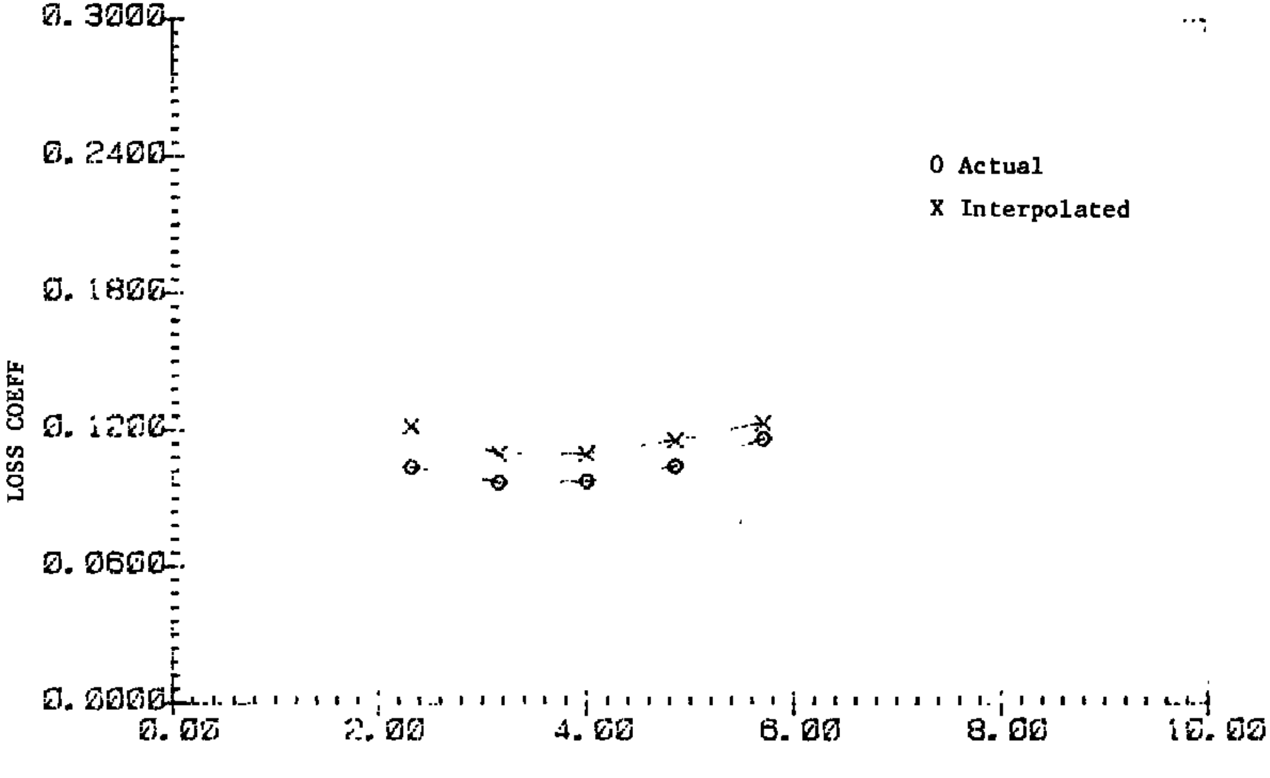

Figure 27. Actual and interpolated curves of total pressure loss coefficient versus angle of incidence (Rotor 4).

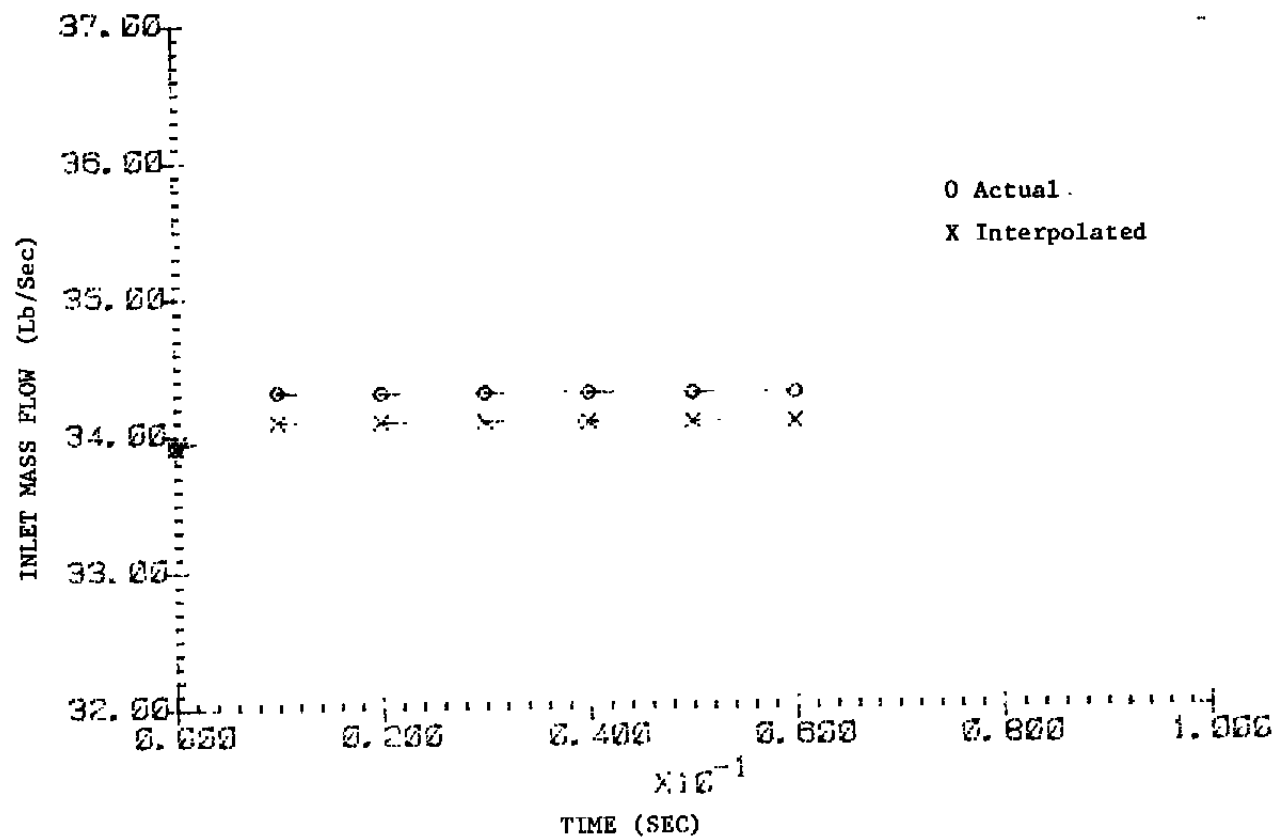

Figure 28. Actual and interpolated (i vs δ and i vs ω) curves of inlet mass flow versus time as the steady state is reached.

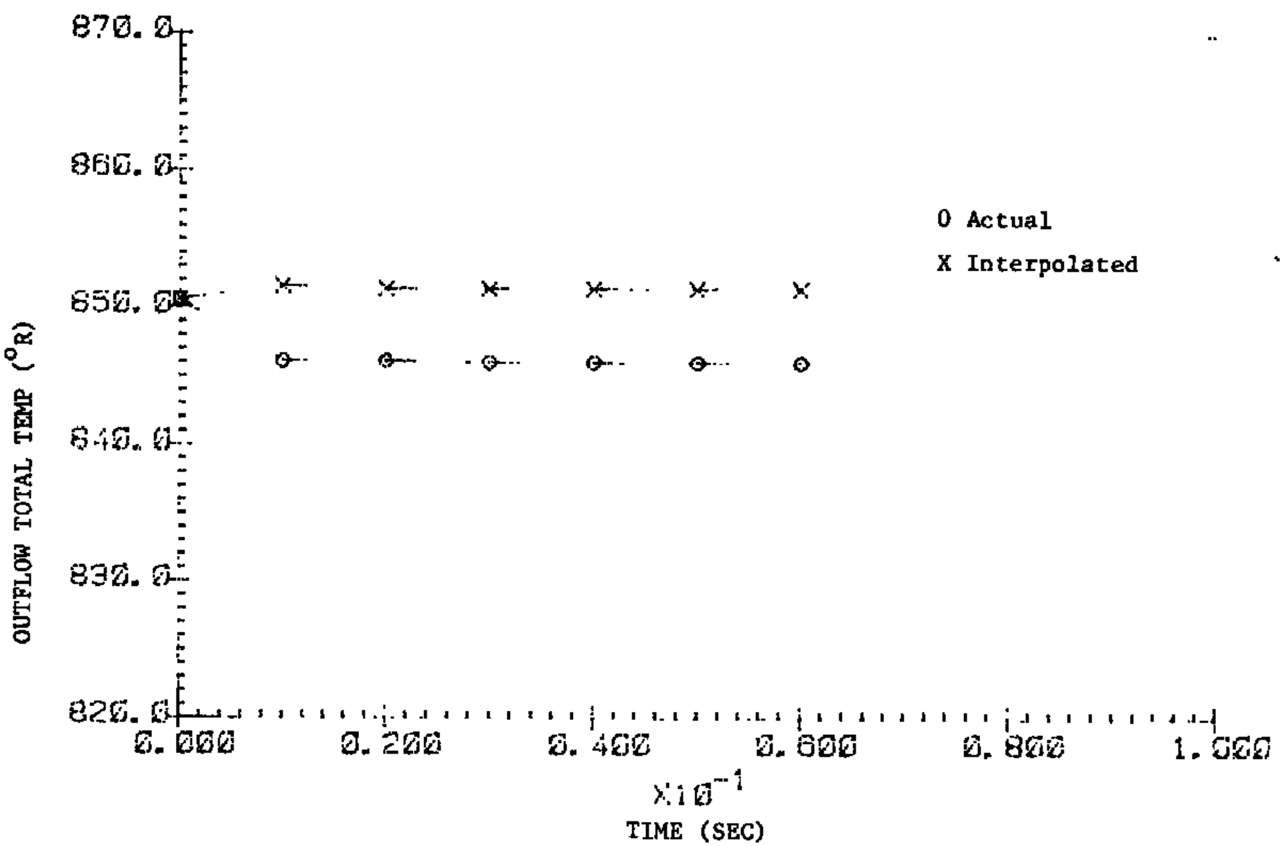

Figure 29. Actual and interpolated (i vs δ and i vs ω) curves of outflow total temperature with time as the steady state is reached.

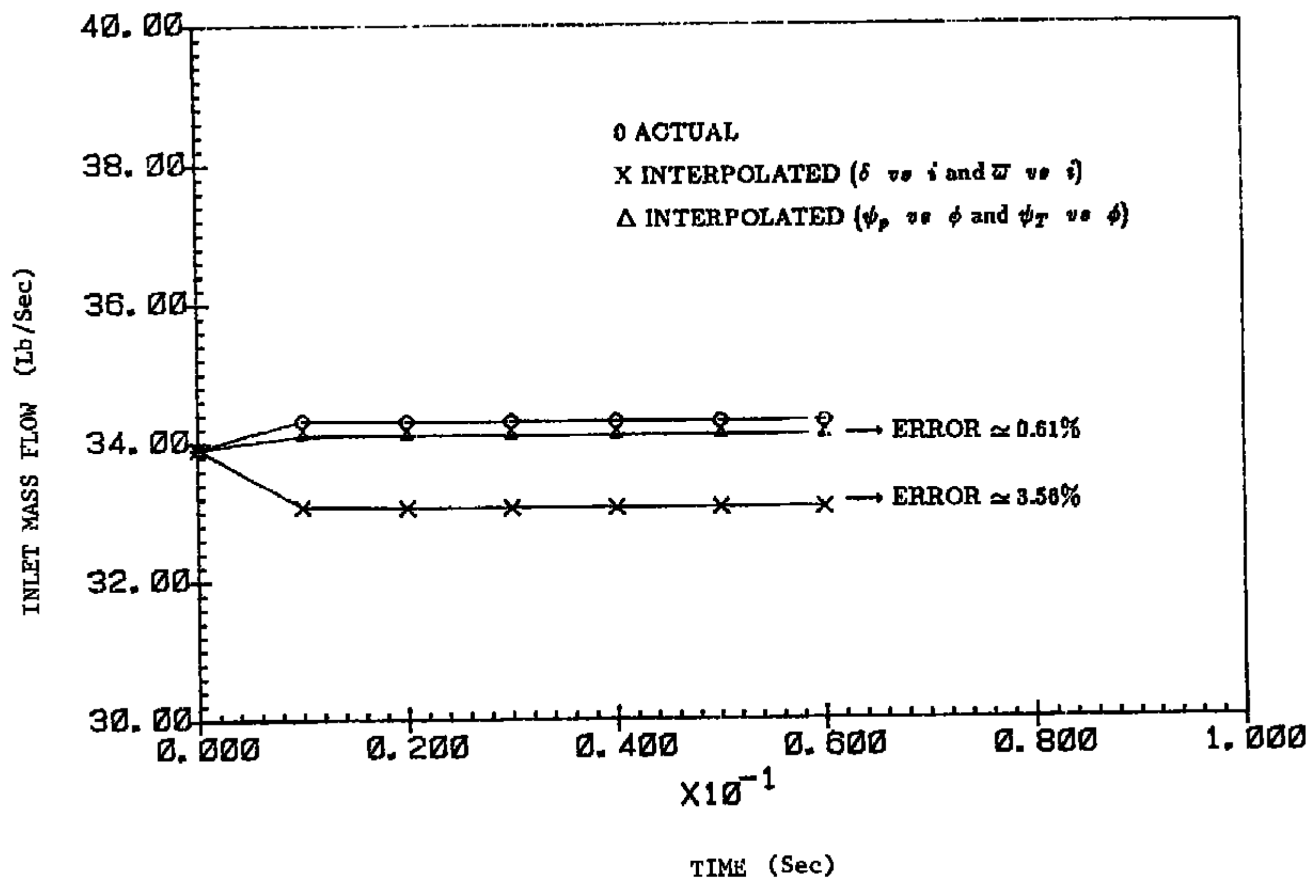

Figure 30. Actual and interpolated (δ and $\overline{\omega}$ vs i) and (ψ_p and ψ_t vs ϕ) curves of inlet mass flow with time as the steady state is reached.

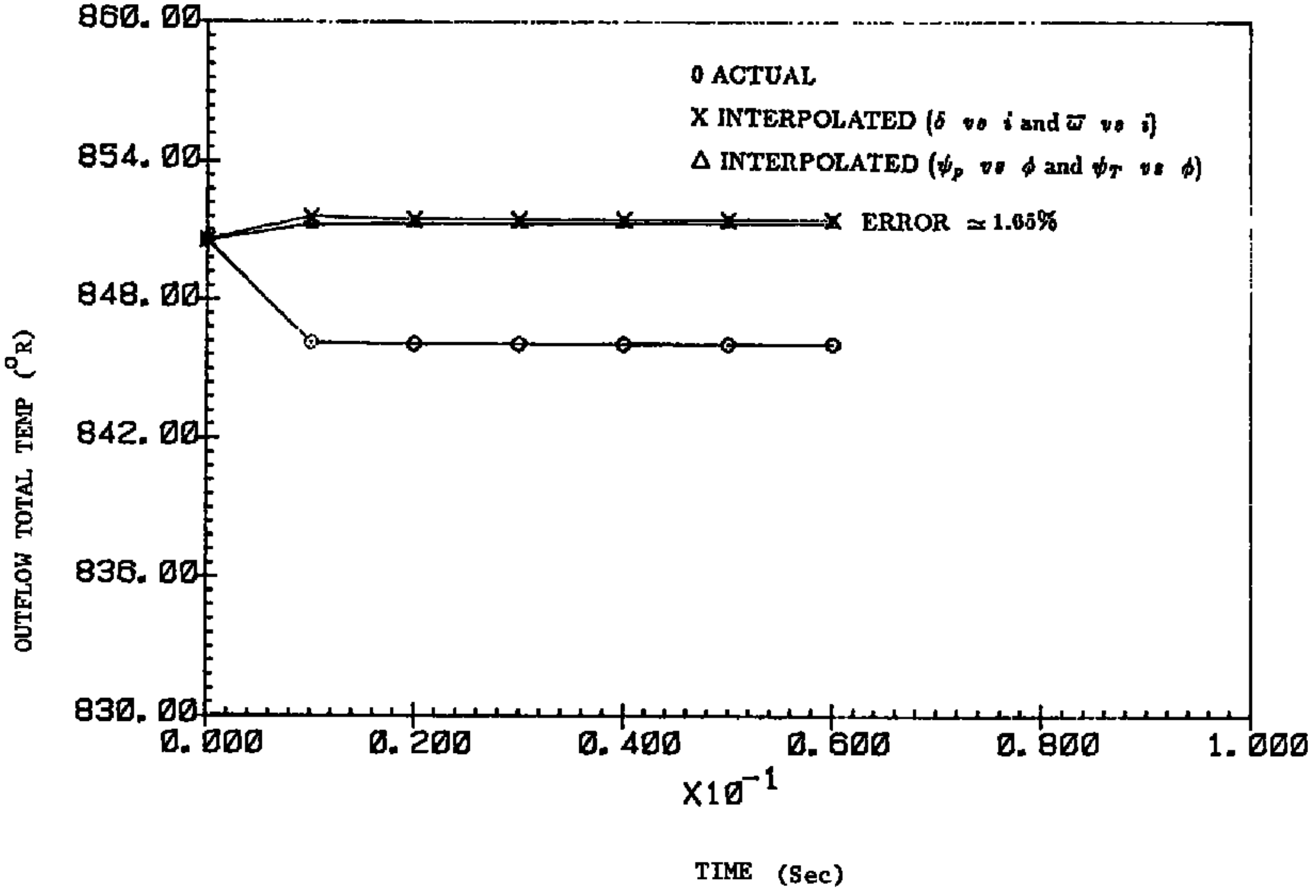

Figure 31. Actual and interpolated (δ and $\bar{\omega}$ vs i) and (ψ_p and ψ_t vs ϕ) curves of outflow total temperature with time as the steady state is reached

APPENDIX A

CHARACTERISTICS AND COMPATIBILITY EQUATIONS

Equation (21) can be rewritten as,

$$\frac{\partial u}{\partial \tilde{u}} \cdot \frac{\partial \tilde{u}}{\partial t} + \frac{\partial f_1}{\partial \tilde{u}} \cdot \frac{\partial \tilde{u}}{\partial z} + \frac{\partial f_2}{\partial \tilde{u}} \cdot \frac{\partial \tilde{u}}{\partial \theta} + \frac{\partial f_2}{\partial r} \cdot \frac{\partial r}{\partial \theta} + g = 0$$

Substituting for $\frac{\partial u}{\partial \tilde{u}}, \frac{\partial f_1}{\partial \tilde{u}}, \frac{\partial f_2}{\partial \tilde{u}}$ and $\frac{\partial f_2}{\partial r}$ we obtain,

$$\frac{\partial \bar{p}}{\partial t} + \left(w\frac{\partial \bar{p}}{\partial z} + \bar{p}\frac{\partial w}{\partial z}\right) + \left(\frac{v}{r}\frac{\partial \bar{p}}{\partial \theta} + \frac{\bar{p}}{r}\frac{\partial v}{\partial \theta}\right) - \frac{\bar{p}v}{r^2} \cdot \frac{\partial r}{\partial \theta} + g_1 = 0$$

$$\left(w\frac{\partial \bar{p}}{\partial t} + \bar{p}\frac{\partial w}{\partial t}\right) - \left(w^2\frac{\partial \bar{p}}{\partial z} + 2\bar{p}w\frac{\partial w}{\partial z} - \frac{\partial \bar{p}}{\partial z}\right) + \left(\frac{vw}{r}\frac{\partial \bar{p}}{\partial \theta} + \frac{\bar{p}v}{r}\frac{\partial w}{\partial \theta}\right.$$
$$\left. + \frac{\bar{p}w}{r}\frac{\partial v}{\partial \theta}\right) - \bar{p}\frac{vw}{r^2}\frac{\partial r}{\partial \theta} + g_2 = 0$$

$$\left(v\frac{\partial \bar{p}}{\partial t} - \bar{p}\frac{\partial v}{\partial t}\right) - \left(wv\frac{\partial \bar{p}}{\partial z} + \bar{p}v\frac{\partial w}{\partial z} - \bar{p}w\frac{\partial v}{\partial z}\right) + \left(\frac{v^2}{r}\frac{\partial \bar{p}}{\partial \theta} + \frac{2\bar{p}v}{r}\frac{\partial v}{\partial \theta} + \frac{1}{r}\frac{\partial \bar{p}}{\partial \theta}\right)$$
$$-\left(\frac{\bar{p}v^2}{r^2} + \frac{\bar{p}}{r^2}\right)\frac{\partial r}{\partial \theta} + g_3 = 0$$

and,

$$\left(\frac{V^2}{2}\frac{\partial \bar{p}}{\partial t} + \bar{p}w\frac{\partial w}{\partial t} + \bar{p}v\frac{\partial v}{\partial t} + \frac{1}{\gamma - 1}\frac{\partial \bar{p}}{\partial t}\right) + \left[w\frac{V^2}{2}\frac{\partial \bar{p}}{\partial z} + \left\{\frac{\gamma \bar{p}}{\gamma - 1} + \bar{p}\left(\frac{V^2}{2} + w^2\right)\right\}\right.$$
$$\left.\frac{\partial w}{\partial z} + \bar{p}wv\frac{\partial v}{\partial z} + \frac{\gamma w}{\gamma - 1}\frac{\partial \bar{p}}{\partial z}\right] + \left[\frac{vV^2}{2r}\frac{\partial \bar{p}}{\partial \theta} + \frac{\bar{p}vw}{r}\frac{\partial w}{\partial \theta} + \left\{\frac{\gamma \bar{p}}{(\gamma - 1)r} + \frac{\bar{p}}{r}\left(\frac{V^2}{2} + v^2\right)\right\}\right.$$
$$\left.\frac{\partial v}{\partial \theta} + \frac{\gamma}{\gamma - 1}\frac{v}{r}\frac{\partial \bar{p}}{\partial \theta}\right] - \left(\frac{\gamma}{\gamma - 1}\frac{v\bar{p}}{r^2} + \frac{\bar{p}}{r^2}\frac{v}{2}V^2\right)\frac{\partial r}{\partial \theta} + g_4 = 0$$

The above equations can be written as,

$$L\frac{\partial \tilde{u}}{\partial t} + N_1\frac{\partial \tilde{u}}{\partial z} + N_2\frac{\partial \tilde{u}}{\partial \theta} + N_3\frac{\partial r}{\partial \theta} + g = 0$$

or,

$$\frac{\partial \tilde{u}}{\partial t} + L^{-1}N_1\frac{\partial \tilde{u}}{\partial z} + L^{-1}N_2\frac{\partial \tilde{u}}{\partial \theta} + L^{-1}N_3\frac{\partial r}{\partial \theta} + L^{-1}g = 0$$

where,

$$L = \frac{\partial u}{\partial \tilde{u}} = \begin{pmatrix} 1 & 0 & 0 & 0 \\ w & \bar{p} & 0 & 0 \\ v & 0 & \bar{p} & 0 \\ \frac{V^2}{2} & \bar{p}w & \bar{p}v & \frac{1}{\gamma - 1} \end{pmatrix}$$

$$L^{-1} = \begin{pmatrix} 1 & 0 & 0 & 0 \\ -\frac{w}{\bar\rho} & \frac{1}{\bar\rho} & 0 & 0 \\ -\frac{v}{\bar\rho} & 0 & \frac{1}{\bar\rho} & 0 \\ \frac{(\gamma-1)V^2}{2} & -(\gamma-1)w & -(\gamma-1)v & (\gamma-1) \end{pmatrix}$$

Let, $\tilde{M}_1 = L^{-1}N_1 = L^{-1}\frac{\partial f_1}{\partial \bar u}$

$$\tilde{M}_1 = \begin{pmatrix} 1 & 0 & 0 & 0 \\ -\frac{w}{\bar\rho} & \frac{1}{\bar\rho} & 0 & 0 \\ -\frac{v}{\bar\rho} & 0 & \frac{1}{\bar\rho} & 0 \\ \frac{(\gamma-1)}{2}V^2 & -(\gamma-1)w & -(\gamma-1)v & (\gamma-1) \end{pmatrix} \begin{pmatrix} w & \bar\rho & 0 & 0 \\ w^2 & 2\bar\rho w & 0 & 1 \\ wv & \bar\rho v & \bar\rho w & 0 \\ \frac{wV^2}{2} & \frac{\gamma\bar p}{\gamma-1} + \bar\rho(\frac{V^2}{2} + w^2) & \bar\rho wv & \frac{\gamma w}{\gamma-1} \end{pmatrix}$$

$$\tilde{M}_1 = \begin{pmatrix} w & \bar\rho & 0 & 0 \\ 0 & w & 0 & \frac{1}{\bar\rho} \\ 0 & 0 & w & 0 \\ 0 & \gamma\bar p & 0 & w \end{pmatrix}$$

For the $\tilde{M}_1$ matrix, the characteristic equation is given by $\mid \tilde{M}_1 - \lambda I \mid = 0$

$$\mid \tilde{M}_1 - \lambda I \mid = \begin{vmatrix} w-\lambda & \bar\rho & 0 & 0 \\ 0 & w-\lambda & 0 & \frac{1}{\bar\rho} \\ 0 & 0 & w-\lambda & 0 \\ 0 & \gamma\bar p & 0 & w-\lambda \end{vmatrix} = 0$$

Solving the above we obtain the roots as.

$$\lambda_1 = w,\ \lambda_2 = w,\ \lambda_3 = w - c,\ \lambda_4 = w - c$$

where $\gamma\bar p/\bar\rho = c^2$

The matrix T formed by the above eigen vectors is,

$$T = \begin{pmatrix} 1 & 0 & 1 & 1 \\ 0 & 0 & \frac{c}{\bar\rho} & \frac{-c}{\bar\rho} \\ 0 & -1 & 0 & 0 \\ 0 & 0 & c^2 & c^2 \end{pmatrix}$$

$$T^{-1} = \begin{pmatrix} 1 & 0 & 0 & -\frac{1}{c^2} \\ 0 & 0 & -1 & 0 \\ 0 & \frac{\bar{\rho}}{2c} & 0 & \frac{1}{2c^2} \\ 0 & -\frac{\bar{\rho}}{2c} & 0 & \frac{1}{2c^2} \end{pmatrix}$$

Also,

$$T^{-1}\tilde{M}_1 T = \begin{pmatrix} w & 0 & 0 & 0 \\ 0 & w & 0 & 0 \\ 0 & 0 & w+c & 0 \\ 0 & 0 & 0 & w-c \end{pmatrix} \;, \quad \text{diagonalizes} \quad \tilde{M}_1$$

Now,

$$\tilde{M}_2 = L^{-1}N_2 = L^{-1}\frac{\partial f_2}{\partial \tilde{u}}$$

$$\tilde{M}_2 = \begin{pmatrix} \frac{v}{r} & 0 & \frac{\bar{\rho}}{r} & 0 \\ 0 & \frac{v}{r} & 0 & 0 \\ 0 & 0 & \frac{v}{r} & \frac{1}{\bar{\rho} r} \\ 0 & 0 & \frac{\gamma \bar{p}}{r} & \frac{v}{r} \end{pmatrix}$$

Similarly,

$$\tilde{M}_3 = L^{-1}N_3 = L^{-1}\frac{\partial f_2}{\partial r} = -\frac{1}{r^2}\begin{pmatrix} \bar{\rho} v \\ 0 \\ \bar{p}/\bar{\rho} \\ 0 \end{pmatrix}$$

$$\tilde{g} = L^{-1}g = \begin{pmatrix} 1 & 0 & 0 & 0 \\ \frac{-w}{\bar{\rho}} & \frac{1}{\bar{\rho}} & 0 & 0 \\ \frac{-v}{\bar{\rho}} & 0 & \frac{1}{\bar{\rho}} & 0 \\ \frac{(\gamma-1)}{2}V^2 & -(\gamma-1)w & -(\gamma-1)v & (\gamma-1) \end{pmatrix} \begin{pmatrix} g_1 \\ g_2 \\ g_3 \\ g_4 \end{pmatrix}$$

$$\begin{aligned} \tilde{g}_1 &= g_1 \\ \tilde{g}_2 &= -\frac{w}{\bar{\rho}}g_1 + \frac{1}{\bar{\rho}}g_2 \\ \tilde{g}_3 &= \frac{-v}{\rho}g_1 + \frac{g_3}{\rho} \\ \tilde{g}_4 &= \frac{(\gamma-1)}{2}V^2 g_1 - (\gamma-1)\left\{ wg_2 + vg_3 - g_4 \right\} \end{aligned}$$

We have,

$$\frac{\partial \tilde{u}}{\partial t} + \tilde{M}_1\frac{\partial \tilde{u}}{\partial z} + \tilde{M}_2\frac{\partial \tilde{u}}{\partial \theta} - \tilde{M}_3\frac{\partial r}{\partial \theta} + \tilde{g} = 0$$

multiplying by T^{-1},

$$T^{-1}\frac{\partial \tilde{u}}{\partial t} + T^{-1}\tilde{M}_1\frac{\partial \tilde{u}}{\partial z} + T^{-1}\tilde{M}_2\frac{\partial \tilde{u}}{\partial \theta} + T^{-1}\tilde{M}_3\frac{\partial r}{\partial \theta} + T^{-1}g = 0$$

$$T^{-1}\frac{\partial \tilde{u}}{\partial t} = \begin{pmatrix} \frac{\partial \bar{\rho}}{\partial t} - \frac{1}{c^2}\frac{\partial \bar{p}}{\partial t} \\ \frac{-\partial v}{\partial t} \\ \frac{\bar{\rho}}{2c}\frac{\partial w}{\partial t} + \frac{1}{2c^2}\frac{\partial \bar{p}}{\partial t} \\ \frac{-\bar{\rho}}{2c}\frac{\partial w}{\partial t} + \frac{1}{2c^2}\frac{\partial \bar{p}}{\partial t} \end{pmatrix}$$

Now, $T^{-1}\tilde{M}_1 T = D$ or $T^{-1}\tilde{M}_1 = DT^{-1}$

$$DT^{-1}\frac{\partial \tilde{u}}{\partial z} = \begin{pmatrix} w\frac{\partial \bar{\rho}}{\partial z} - \frac{w}{c^2}\frac{\partial \bar{p}}{\partial z} \\ -w\frac{\partial v}{\partial z} \\ \frac{\bar{\rho}}{2c}(w+c)\frac{\partial w}{\partial z} + \frac{1}{2c^2}(w+c)\frac{\partial \bar{p}}{\partial z} \\ \frac{-\bar{\rho}}{2c}(w-c)\frac{\partial w}{\partial z} + \frac{1}{2c^2}(w-c)\frac{\partial \bar{p}}{\partial z} \end{pmatrix}$$

Now,

$$T^{-1}\tilde{M}_2\frac{\partial \tilde{u}}{\partial \theta} = \begin{pmatrix} \frac{v}{r}\frac{\partial \bar{\rho}}{\partial \theta} - \frac{v}{c^2 r}\frac{\partial \bar{p}}{\partial \theta} \\ \frac{-v}{r}\frac{\partial v}{\partial \theta} - \frac{1}{\bar{\rho} r}\frac{\partial \bar{p}}{\partial \theta} \\ \frac{\bar{\rho} v}{2cr}\frac{\partial w}{\partial \theta} + \frac{\bar{\rho}}{2r}\frac{\partial v}{\partial \theta} + \frac{v}{2c^2 r}\frac{\partial \bar{p}}{\partial \theta} \\ \frac{-\bar{\rho} v}{2cr}\frac{\partial w}{\partial \theta} - \frac{\bar{\rho}}{2r}\frac{\partial v}{\partial \theta} + \frac{v}{2c^2 r}\frac{\partial \bar{p}}{\partial \theta} \end{pmatrix}$$

$$T^{-1}\tilde{M}_3\frac{\partial r}{\partial \theta} = \begin{pmatrix} -\frac{\bar{\rho} v}{r^2}\frac{\partial r}{\partial \theta} \\ \frac{c^2}{\gamma r^2}\frac{\partial r}{\partial \theta} \\ 0 \\ 0 \end{pmatrix}$$

$$T^{-1}\tilde{g} = \begin{pmatrix} \tilde{g}_1 - \frac{\tilde{g}_4}{c^2} \\ -\tilde{g}_3 \\ \frac{\bar{\rho}}{2c}\tilde{g}_2 + \frac{1}{2c^2}\tilde{g}_4 \\ \frac{-\bar{\rho}}{2c}\tilde{g}_2 + \frac{1}{2c^2}\tilde{g}_4 \end{pmatrix}$$

substituting the above, the compatibility equations are derived as.

$$\frac{\partial \bar{\rho}}{\partial t} - \frac{1}{c^2}\frac{\partial \bar{p}}{\partial t} + w\frac{\partial \bar{\rho}}{\partial Z} - \frac{w}{c^2}\frac{\partial \bar{p}}{\partial Z} + \frac{v}{r}\left(\frac{\partial \bar{\rho}}{\partial \theta} - \frac{1}{c^2}\frac{\partial \bar{p}}{\partial \theta}\right)$$

$$-\frac{\bar{\rho} v}{r^2}\frac{\partial r}{\partial \theta} + \tilde{g}_1 - \frac{\tilde{g}_4}{c^2} = 0$$

$$\left(\frac{\partial}{\partial t} + w\frac{\partial}{\partial Z}\right)\bar{\rho} - \frac{1}{c^2}\left(\frac{\partial}{\partial t} + w\frac{\partial}{\partial Z}\right)\bar{p} - \frac{v}{r}\left(\frac{\partial \bar{\rho}}{\partial \theta} - \frac{1}{c^2}\frac{\partial \bar{p}}{\partial \theta}\right)$$

$$-\frac{\bar{\rho} v}{r^2}\frac{\partial r}{\partial \theta} + \tilde{g}_1 - \frac{\tilde{g}_4}{c^2} = 0$$

or

$$\frac{d\bar{p}}{dt} - \frac{1}{c^2}\frac{d\bar{p}}{dt} + \frac{v}{r}\left(\frac{\partial \bar{p}}{\partial \theta} - \frac{1}{c^2}\frac{\partial \bar{p}}{\partial \theta}\right) - \frac{\bar{\rho} v}{r^2}\frac{\partial r}{\partial \theta} + \bar{g}_1 - \frac{\tilde{g}_4}{c^2} = 0,$$

$$\text{along } \frac{dZ}{dt} = w \text{ for a fixed } \theta. \qquad (A.1)$$

$$-\frac{\partial v}{\partial t} - w\frac{\partial v}{\partial Z} - \frac{1}{r}\left(v\frac{\partial v}{\partial \theta} + \frac{1}{\bar{\rho}}\frac{\partial \bar{p}}{\partial \theta}\right) + \frac{c^2}{\gamma r^2}\frac{\partial r}{\partial \theta} - \tilde{g}_3 = 0$$

or

$$\frac{dv}{dt} - \frac{1}{r}\left(v\frac{\partial v}{\partial \theta} + \frac{1}{\bar{\rho}}\frac{\partial \bar{p}}{\partial \theta}\right) - \frac{c^2}{\gamma r^2}\frac{\partial r}{\partial \theta} + \tilde{g}_3 = 0.$$

$$\text{along } \frac{dZ}{dt} = w \text{ for a fixed } \theta. \qquad (A.2)$$

$$\frac{\bar{\rho}}{2c}\left(\frac{\partial}{\partial t} + (w + c)\frac{\partial}{\partial Z}\right)w - \frac{1}{2c^2}\left(\frac{\partial}{\partial t} + (w + c)\frac{\partial}{\partial Z}\right)\bar{p} - \frac{\bar{\rho}}{r}\left(\frac{v}{2c}\frac{\partial w}{\partial \theta} + \frac{1}{2}\frac{\partial v}{\partial \theta}\right)$$

$$+\frac{v}{2c^2 r}\frac{\partial \bar{p}}{\partial \theta} + \frac{\bar{\rho}}{2c}\tilde{g}_2 + \frac{1}{2c^2}\tilde{g}_4 = 0$$

or

$$\frac{dw}{dt} + \frac{1}{\bar{\rho} c}\frac{d\bar{p}}{dt} + \frac{v}{r}\frac{\partial w}{\partial \theta} + \frac{c}{r}\frac{\partial v}{\partial \theta} + \frac{v}{\bar{\rho} c r}\frac{\partial \bar{p}}{\partial \theta} + \tilde{g}_2 + \frac{1}{\bar{\rho} c}\tilde{g}_4 = 0,$$

$$\text{along } \frac{dZ}{dt} = w + c \text{ for a fixed } \theta. \qquad (A.3)$$

$$\frac{-\bar{\rho}}{2c}\left(\frac{\partial}{\partial t} + (w - c)\frac{\partial}{\partial z}\right)w - \frac{1}{2c^2}\left(\frac{\partial}{\partial t} + (w - c)\frac{\partial}{\partial z}\right)\bar{p} - \frac{\bar{\rho} v}{2cr}\frac{\partial w}{\partial \theta} + \frac{\bar{\rho}}{2r}\frac{\partial v}{\partial \theta}$$

$$-\frac{v}{2c^2 r}\frac{\partial \bar{p}}{\partial \theta} - \frac{\bar{\rho}}{2c}\tilde{g}_2 - \frac{1}{2c^2}\tilde{g}_4 = 0$$

or

$$\frac{dw}{dt} - \frac{1}{\bar{\rho} c}\frac{d\bar{p}}{dt} - \frac{v}{r}\frac{\partial w}{\partial \theta} - \frac{c}{r}\frac{\partial v}{\partial \theta} - \frac{v}{\bar{\rho} c r}\frac{d\bar{p}}{d\theta} + \tilde{g}_2 - \frac{1}{\bar{\rho} c}\tilde{g}_4 = 0,$$

$$\text{along } \frac{dz}{dt} = w - c \text{ for a fixed } \theta. \qquad (A.4)$$

NOMENCLATURE

A	Area
ρ	density
e	internal energy
P	static pressure, matrix as defined in Chapter 5
P_t	total pressure
c_p	specific heat at constant pressure
c_v	specific heat at constant volume
γ	ratio of specific heats
T	static temperature, matrix as defined in Appendix A
T_t	total temperature
W_B	compressor bleed flow rate
t	time
F	force of compressor blading and casing friction acting on fluid
W_s	stage shaft work added to fluid in control volume
R	gas constant
x, y, z	coordinates in the cartesian coordinate system
c	speed of sound
CN	courant number
$\vec{u}$	as defined in Eq. (2)
$\vec{f}$	as defined in Eq. (2)
$\vec{g}$	as defined in Eq. (2), and Eq. (21)
IMP	impulse function

N	number of time steps, *rpm* of engine
ϕ	flow coefficient
ψ_p	pressure coefficient
ψ_t	temperature coefficient
i	angle of incidence
δ	deviation angle
V	absolute velocity, volume, total velocity
V'	velocity
r	radius at pitchline
β	absolute flow angle
β'	relative flow angle
$\bar{\omega}$	total pressure loss coefficient
M_a	axial Mach number
M_T	rotor Mach number at pitch radius
r_1	hub radius
r_2	tip radius
r, θ, z	cylindrical polar coordinates
u, v, w	components of velocity in the radial, circumferential, and axial directions, respectively
$\vec{f}_1, \vec{f}_2$	as defined in Eq. (21)
M_1, M_2	Jacobian matrices as defined in Eq. (22), matrices as defined in Appendix A

Ω	rotor angular velocity
$-$	averaged values in radial direction
L	length, matrix as defined in Appendix A
M	Mach number
H	total enthalpy
$N_1, N_2, N3$	matrices as defined in Appendix A
$\lambda_{1,2,3,4}$	roots of the characteristic equation
q	as defined in Section 5
Q	rate of heat addition
k_1, k_2	arbitrary constants

SUBSCRIPTS

'r'	refers to rotor, radial direction
's'	refers to stator
'0'	in front of the stator
'1'	after the stator and in front of the rotor
'2'	after the rotor
'θ'	refers to circumferential direction
'z'	refers to axial direction

SUPERSCRIPTS

$'$	variables with respect to rotor coordinates
$+$	refers to values at the forward node
$-$	values at the previous node
$\sim$	as defined in Appendix A